EQUIFORMER: EQUIVARIANT GRAPH ATTENTION TRANSFORMER FOR 3D ATOMISTIC GRAPHS

Anonymous authors
Paper under double-blind review

ABSTRACT

3D-related inductive biases like translational invariance and rotational equivariance are indispensable to learning on 3D atomistic graphs such as molecules. Inspired by the success of Transformers in various domains, we study how to incorporate these inductive biases into Transformers. In this paper, we present Equiformer, a graph neural network leveraging the strength of Transformer architectures and incorporating $SE(3)/E(3)$-equivariant features based on irreducible representations (irreps). Irreps features encode equivariant information in channels without complicating graph structures and thus enable us to directly incorporate them into Transformers by using equivariant operations. Moreover, we propose a novel attention mechanism called equivariant graph attention, which considers both content and geometric information contained in irreps features. The proposed equivariant graph attention improves upon typical attention in Transformers through replacing dot product attention with multi-layer perceptron attention and including non-linear message passing. We benchmark Equiformer on QM9, MD17, and OC20 datasets. Experiments demonstrate that Equiformer achieves competitive results to previous models and verify the effectiveness of the proposed attention.

1 INTRODUCTION

Machine learned models can accelerate the prediction of quantum properties of atomistic systems like molecules by learning approximations of *ab initio* calculations (Gilmer et al., 2017; Zhang et al., 2018b; Jia et al., 2020; Gasteiger et al., 2020a; Batzner et al., 2022; Lu et al., 2021; Unke et al., 2021; Sriram et al., 2022; Rackers et al., 2022). In particular, graph neural networks (GNNs) have gained increasing popularity due to their performance. By modeling atomistic systems as graphs, GNNs naturally treat the set-like nature of collections of atoms, encode the interaction between atoms in node features and update the features by passing messages between nodes. One factor contributing to the success of neural networks is the ability to incorporate inductive biases that exploit the symmetry of data. Take convolutional neural networks (CNNs) for 2D images as an example: Patterns in images should be recognized regardless of their positions, which motivates the inductive bias of translational equivariance. As for atomistic graphs, where each atom has its coordinate in 3D Euclidean space, we consider inductive biases related to 3D Euclidean group $E(3)$, which include equivariance to 3D translation, 3D rotation, and inversion. Concretely, some properties like energy of an atomistic system should be constant regardless of how we shift the system; others like force should be rotated accordingly if we rotate the system. To incorporate these inductive biases, equivariant and invariant neural networks have been proposed. The former leverages geometric tensors like vectors for equivariant node features (Thomas et al., 2018; Weiler et al., 2018; Kondor et al., 2018; Fuchs et al., 2020; Batzner et al., 2022; Brandstetter et al., 2022; Musaelian et al., 2022), and the latter augments graphs with invariant information such as distances and angles extracted from 3D graphs (Schütt et al., 2017; Gasteiger et al., 2020b;a; Liu et al., 2022; Klicpera et al., 2021).

A parallel line of research focuses on applying Transformer networks (Vaswani et al., 2017) to other domains like computer vision (Carion et al., 2020; Dosovitskiy et al., 2021; Touvron et al., 2020) and graph (Dwivedi & Bresson, 2020; Kreuzer et al., 2021; Ying et al., 2021; Shi et al., 2022) and has demonstrated widespread success. However, as Transformers were developed for sequence data (Devlin et al., 2019; Baevski et al., 2020; Brown et al., 2020), it is crucial to incorporate domain-related inductive biases. For example, Vision Transformer (Dosovitskiy et al., 2021) shows that adopting a pure Transformer to image classification cannot generalize well and achieves worse results than CNNs when trained on only ImageNet (Russakovsky et al., 2015) since it lacks inductive

biases like translational invariance. Note that ImageNet contains over 1.28M images and the size is already larger than that of many quantum properties prediction datasets (Ruddigkeit et al., 2012; Chmiela et al., 2017; Chanussot* et al., 2021). Therefore, this highlights the necessity of including correct inductive biases when applying Transformers to the domain of 3D atomistic graphs.

In this work, we present **Equiformer**, an equivariant graph neural network utilizing $SE(3)$/$E(3)$-**equi**variant features built from irreducible representations (irreps) and a novel attention mechanism to combine the 3D-related inductive bias with the strength of Trans**former**. Irreps features encode equivariant information in channels without complicating graph structures. The simplicity enables us to directly incorporate them into Transformers through replacing original operations with equivariant counterparts and introducing an additional equivariant operation called tensor product. Moreover, we propose a novel attention mechanism called equivariant graph attention, which considers both content and geometric information such as relative position. The proposed attention improves upon typical attention in Transformers by replacing dot product attention with theoretically stronger multi-layer perceptron attention and including non-linear message passing.

With these innovations, Equiformer achieves competitive results on QM9 (Ruddigkeit et al., 2012; Ramakrishnan et al., 2014), MD17 (Chmiela et al., 2017; Schütt et al., 2017; Chmiela et al., 2018) and OC20 (Chanussot* et al., 2021) datasets. For QM9 and MD17, Equiformer achieves overall better results across all tasks or all molecules compared to previous models like NequIP (Batzner et al., 2022), PaiNN (Schütt et al., 2021) and TorchMD-NET (Thölke & Fabritiis, 2022). For OC20, when trained with IS2RE data and optionally IS2RS data, Equiformer improves upon state-of-the-art models such as SEGNN (Brandstetter et al., 2022) and Graphormer (Shi et al., 2022). Particularly, as of the submission of this work, Equiformer achieves the best IS2RE result when only IS2RE and IS2RS data are used and improves training time by $2.3\times$ to $15.5\times$ compared to previous models.

2 Related Works

Here, we focus on equivariant neural networks and discuss other works in Sec. B in appendix.

***SE(3)/E(3)*-Equivariant GNNs.** Equivariant neural networks (Thomas et al., 2018; Kondor et al., 2018; Weiler et al., 2018; Fuchs et al., 2020; Miller et al., 2020; Townshend et al., 2020; Batzner et al., 2022; Jing et al., 2021; Schütt et al., 2021; Satorras et al., 2021; Unke et al., 2021; Brandstetter et al., 2022; Thölke & Fabritiis, 2022; Le et al., 2022; Musaelian et al., 2022) operate on geometric tensors like type-L vectors to achieve equivariance. The central idea is to use functions of geometry built from spherical harmonics and irreps features to achieve 3D rotational and translational equivariance as proposed in Tensor Field Network (TFN) (Thomas et al., 2018), which generalizes 2D counterparts (Worrall et al., 2016; Cohen & Welling, 2016; Cohen et al., 2018) to 3D Euclidean space (Thomas et al., 2018; Weiler et al., 2018; Kondor et al., 2018). Previous works differ in equivariant operations used in their networks. TFN (Thomas et al., 2018) and NequIP (Batzner et al., 2022) use graph convolution with linear messages, with the latter utilizing extra equivariant gate activations (Weiler et al., 2018). SEGNN (Brandstetter et al., 2022) introduces non-linear messages (Gilmer et al., 2017; Sanchez-Gonzalez et al., 2020) for irreps features, and the non-linear messages use the same gate activation and improve upon linear messages. SE(3)-Transformer (Fuchs et al., 2020) adopts an equivariant version of dot product (DP) attention (Vaswani et al., 2017) with linear messages, and the attention can support vectors of any type L. Subsequent works on equivariant Transformers (Thölke & Fabritiis, 2022; Le et al., 2022) follow the practice of DP attention and linear messages but use more specialized architectures considering only type-0 and type-1 vectors.

The proposed Equiformer incorporates all the advantages through combining MLP attention with non-linear messages and supporting vectors of any type. Compared to TFN, NequIP, SEGNN and SE(3)-Transformer, the proposed combination of MLP attention and non-linear messages is more expressive than pure linear or non-linear messages and pure MLP or dot product attention. Compared to other equivariant Transformers (Thölke & Fabritiis, 2022; Le et al., 2022), in addition to being more expressive, the proposed attention mechanism can support vectors of higher degrees (types) and involve higher order tensor product interactions, which can lead to better performance.

3 Background

3.1 $E(3)$ Equivariance

Atomistic systems are often described using coordinate systems. For 3D Euclidean space, we can freely choose coordinate systems and change between them via the symmetries of 3D space: 3D

translation, rotation and inversion ($\vec{r} \rightarrow -\vec{r}$). The groups of 3D translation, rotation and inversion form Euclidean group $E(3)$, with the first two forming $SE(3)$, the second being $SO(3)$, and the last two forming $O(3)$. The laws of physics are invariant to the choice of coordinate systems and therefore properties of atomistic systems are equivariant, e.g., when we rotate our coordinate system, quantities like energy remain the same while others like force rotate accordingly. Formally, a function f mapping between vector spaces X and Y is equivariant to a group of transformation G if for any input $x \in X$, output $y \in Y$ and group element $g \in G$, we have $f(D_X(g)x) = D_Y(g)f(x)$, where $D_X(g)$ and $D_Y(g)$ are transformation matrices parametrized by g in X and Y. For learning on 3D atomistic graphs, features and learnable functions should be $E(3)$-equivariant to geometric transformation acting on position $\vec{r}$. In this work, following previous works (Thomas et al., 2018; Kondor et al., 2018; Weiler et al., 2018) implemented in `e3nn` (Geiger et al., 2022), we achieve $SE(3)$/$E(3)$-equivariance by using equivariant features based on vector spaces of irreducible representations and equivariant operations for learnable functions. In the main text, we discuss $SE(3)$-equivariance and benchmark Equiformer with $SE(3)$-equivariance. We leave the discussion on inversion and $E(3)$-equivariance in Sec. A and present results of $E(3)$-equivariance in Sec. D.2 and Sec. F.4 in appendix.

3.2 Irreducible Representations

A group representation (Dresselhaus et al., 2007; Zee, 2016) defines transformation matrices $D_X(g)$ of group elements g that act on a vector space X. For 3D Euclidean group $E(3)$, two examples of vector spaces with different transformation matrices are scalars and Euclidean vectors in $\mathbb{R}^3$, i.e., vectors change with rotation while scalars do not. To address translation symmetry, we operate on relative positions. The transformation matrices of rotation and inversion are separable and commute. We discuss irreducible representations of $SO(3)$ below and discuss inversion in Sec. A.3 in appendix.

Any group representation of $SO(3)$ on a given vector space can be decomposed into a concatenation of provably smallest transformation matrices called irreducible representations (irreps). Specifically, for group element $g \in SO(3)$, there are $(2L+1)$-by-$(2L+1)$ irreps matrices $D_L(g)$ called Wigner-D matrices acting on $(2L+1)$-dimensional vector spaces, where degree L is a non-negative integer. L can be interpreted as an angular frequency and determines how quickly vectors change when rotating coordinate systems. $D_L(g)$ of different L act on independent vector spaces. Vectors transformed by $D_L(g)$ are type-L vectors, with scalars and Euclidean vectors being type-0 and type-1 vectors. It is common to index elements of type-L vectors with an index m called order, where $-L \leq m \leq L$.

Irreps Features. We concatenate multiple type-L vectors to form $SE(3)$-equivariant irreps features. Concretely, irreps feature f has C_L type-L vectors, where $0 \leq L \leq L_{max}$ and C_L is the number of channels for type-L vectors. We index irreps features f by channel c, degree L, and order m and denote as $f^{(L)}_{c,m}$. Different channels of type-L vectors are parametrized by different weights but are transformed with the same $D_L(g)$. Regular scalar features correspond to only type-0 vectors.

Spherical Harmonics. Euclidean vectors $\vec{r}$ in $\mathbb{R}^3$ can be projected into type-L vectors $f^{(L)}$ by using spherical harmonics (SH) $Y^{(L)}$: $f^{(L)} = Y^{(L)}(\frac{\vec{r}}{||\vec{r}||})$. SH are $E(3)$-equivariant with $D_L(g)f^{(L)} = Y^{(L)}(\frac{D_1(g)\vec{r}}{||D_1(g)\vec{r}||})$. SH of relative position $\vec{r}_{ij}$ generates the first set of irreps features. Equivariant information propagates to other irreps features through equivariant operations like tensor products.

3.3 Tensor Product

Tensor products can interact different type-L vectors. We discuss tensor products for $SO(3)$ below and those for $O(3)$ in Sec. A.4. The tensor product denoted as $\otimes$ uses Clebsch-Gordan coefficients to combine type-L_1 vector $f^{(L_1)}$ and type-L_2 vector $g^{(L_2)}$ and produces type-L_3 vector $h^{(L_3)}$:

$$h^{(L_3)}_{m_3} = (f^{(L_1)} \otimes g^{(L_2)})_{m_3} = \sum_{m_1=-L_1}^{L_1} \sum_{m_2=-L_2}^{L_2} C^{(L_3,m_3)}_{(L_1,m_1)(L_2,m_2)} f^{(L_1)}_{m_1} g^{(L_2)}_{m_2} \tag{1}$$

where m_1 denotes order and refers to the m_1-th element of $f^{(L_1)}$. Clebsch-Gordan coefficients $C^{(L_3,m_3)}_{(L_1,m_1)(L_2,m_2)}$ are non-zero only when $|L_1 - L_2| \leq L_3 \leq |L_1 + L_2|$ and thus restrict output vectors to be of certain types. For efficiency, we discard vectors with $L > L_{max}$, where L_{max} is a hyper-parameter, to prevent vectors of increasingly higher dimensions.

We call each distinct non-trivial combination of $L_1 \otimes L_2 \rightarrow L_3$ a path. Each path is independently equivariant, and we can assign one learnable weight to each path in tensor products, which is similar

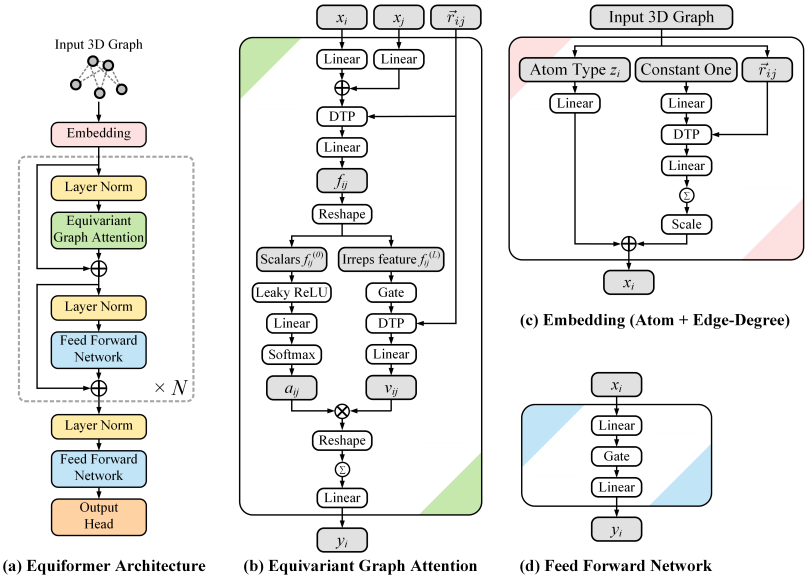

Figure 1: **Architecture of Equiformer.** We embed input 3D graphs with atom and edge-degree embeddings and process them with Transformer blocks, consisting of equivariant graph attention and feed forward networks. In this figure, "$\otimes$" denotes multiplication, "$\oplus$" denotes addition, and "DTP" stands for depth-wise tensor product. $\sum$ within a circle denotes summation over all neighbors. Gray cells indicate intermediate irreps features.

to typical linear layers. We can generalize Eq. 1 to irreps features and include multiple channels of vectors of different types through iterating over all paths associated with channels of vectors. In this way, weights are indexed by $(c_1, l_1, c_2, l_2, c_3, l_3)$, where c_1 is the c_1-th channel of type-l_1 vector in input irreps feature. We use $\otimes_w$ to represent tensor product with weights w. Weights can be conditioned on quantities like relative distances.

4 EQUIFORMER

We incorporate $SE(3)/E(3)$-equivariant irreps features into Transformers (Vaswani et al., 2017) and use equivariant operations. Additionally, we propose a novel attention mechanism called equivariant graph attention. The overall architecture of Equiformer is illustrated in Fig. 1.

4.1 EQUIVARIANT OPERATIONS FOR IRREPS FEATURES

Here we discuss equivariant operations used in Equiformer that serve as building blocks for equivariant graph attention and other modules. They include the equivariant version of the original operations in Transformers and the depth-wise tensor product as illustrated in Fig. 2.

Linear. Linear layers are generalized to irreps features by transforming different type-L vectors separately. Specifically, we apply separate linear operations to each group of type-L vectors. We remove bias terms for non-scalar features with $L > 0$ as biases do not depend on inputs, and therefore, including biases for type-L vectors with $L > 0$ can break equivariance.

Layer Normalization. Transformers adopt layer normalization (LN) (Ba et al., 2016) to stabilize training. Given input $x \in \mathbb{R}^{N \times C}$, with N being the number of nodes and C the number of channels, LN calculates the linear transformation of normalized input as $\text{LN}(x) = \left(\frac{x - \mu_C}{\sigma_C}\right) \circ \gamma + \beta$, where $\mu_C, \sigma_C \in \mathbb{R}^{N \times 1}$ are mean and standard deviation of input x along the channel dimension, $\gamma, \beta \in \mathbb{R}^{1 \times C}$ are learnable parameters, and $\circ$ denotes element-wise product. By viewing standard deviation as the root mean square value (RMS) of L2-norm of type-L vectors, LN can be generalized to irreps features. Specifically, given input $x \in \mathbb{R}^{N \times C \times (2L+1)}$ of type-L vectors, the output is $\text{LN}(x) = \left(\frac{x}{\text{RMS}_C(\text{norm}(x))}\right) \circ \gamma$, where $\text{norm}(x) \in \mathbb{R}^{N \times C \times 1}$ calculates the L2-norm of each type-L vectors in x, and $\text{RMS}_C(\text{norm}(x)) \in \mathbb{R}^{N \times 1 \times 1}$ calculates the RMS of L2-norm with mean taken along the channel dimension. We remove means and biases for type-L vectors with $L \neq 0$.

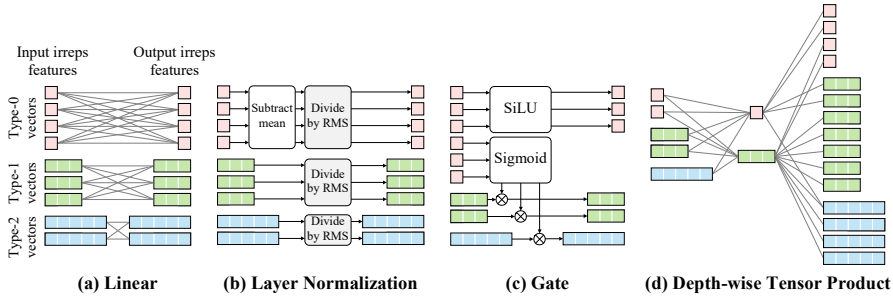

Figure 2: **Equivariant operations used in Equiformer. (a)** Each gray line between input and output irreps features contains one learnable weight. **(b)** "RMS" denotes the root mean square value along the channel dimension. For simplicity, we have removed multiplying by γ here. **(c)** Gate layers are equivariant activation functions where non-linearly transformed scalars are used to gate non-scalar irreps features. **(d)** The left two irreps features correspond to two input irreps features, and the rightmost one is the output irreps feature. The two gray lines connecting two vectors in the input irreps features and one vector in the output irreps feature form a path and contain one learnable weight. An alternative visualization of depth-wise tensor products can be found in Fig. 3 in appendix. We show $SE(3)$-equivariant operations here, which can be generalized to $E(3)$-equivariant features.

Gate. We use the gate activation (Weiler et al., 2018) for equivariant activation function as shown in Fig. 2(c). Typical activation functions are applied to type-0 vectors. For vectors of higher L, we multiply them with non-linearly transformed type-0 vectors for equivariance. Specifically, given input x containing non-scalar C_L type-L vectors with $0 < L \leq L_{max}$ and $(C_0 + \sum_{L=1}^{L_{max}} C_L)$ type-0 vectors, we apply SiLU (Elfwing et al., 2017; Ramachandran et al., 2017) to the first C_0 type-0 vectors and sigmoid function to the other $\sum_{L=1}^{L_{max}} C_L$ type-0 vectors to obtain non-linear weights and multiply each type-L vector with corresponding non-linear weights. After the gate activation, the number of channels for type-0 vectors is reduced to C_0.

Depth-wise Tensor Product. The tensor product defines interaction between vectors of different L. To improve its efficiency, we use the depth-wise tensor product (DTP), where one type-L vector in output irreps features depends only on one type-L' vector in input irreps features as illustrated in Fig. 2(d) and Fig. 3, with L being equal to or different from L'. This is similar to depth-wise convolution (Howard et al., 2017), where one output channel depends on only one input channel. Weights w in the DTP can be input-independent or conditioned on relative distances, and the DTP between two tensors x and y is denoted as $x \otimes_w^{DTP} y$. Note that the one-to-one dependence of channels can significantly reduce the number of weights and thus memory complexity when weights are conditioned on relative distances. In contrast, if one output channel depends on all input channels, in our case, this can lead to out-of-memory errors when weights are parametrized by relative distances.

4.2 Equivariant Graph Attention

Self-attention (Vaswani et al., 2017; Veličković et al., 2018; Fuchs et al., 2020; Khan et al., 2021; Ying et al., 2021; Brody et al., 2022) transforms features sent from one spatial location to another with input-dependent weights. We use the notion from Transformers (Vaswani et al., 2017) and message passing networks (Gilmer et al., 2017) and define message m_{ij} sent from node j to node i as follows:

$$m_{ij} = a_{ij} \times v_{ij} \tag{2}$$

where attention weights a_{ij} depend on features on node i and its neighbors $\mathcal{N}(i)$ and values v_{ij} are transformed with input-independent weights. In Transformers and Graph Attention Networks (GAT) (Veličković et al., 2018; Brody et al., 2022), v_{ij} depends only on node j. In message passing networks (Gilmer et al., 2017), v_{ij} depends on features on nodes i and j with constant a_{ij}. The proposed equivariant graph attention adopts tensor products to incorporate content and geometric information and uses multi-layer perceptron attention for a_{ij} and non-linear message passing for v_{ij} as illustrated in Fig. 1(b).

Incorporating Content and Geometric Information. Given features x_i and x_j on target node i and source node j, we combine the two features with two linear layers to obtain initial message $x_{ij} = \text{Linear}_{dst}(x_i) + \text{Linear}_{src}(x_j)$. x_{ij} is passed to a DTP layer and a linear layer to consider

geometric information like relative position contained in different type-L vectors in irreps features:

$$x'_{ij} = x_{ij} \otimes^{DTP}_{w(||\vec{r}_{ij}||)} \text{SH}(\vec{r}_{ij}) \quad \text{and} \quad f_{ij} = \text{Linear}(x'_{ij}) \tag{3}$$

where x'_{ij} is the tensor product of x_{ij} and spherical harmonics embeddings (SH) of relative position $\vec{r}_{ij}$, with weights parametrized by $||\vec{r}_{ij}||$. f_{ij} considers semantic and geometric features on source and target nodes in a linear manner and is used to derive attention weights and non-linear messages.

Multi-Layer Perceptron Attention. Attention weights a_{ij} capture how each node interacts with neighboring nodes. a_{ij} are invariant to geometric transformation, and thus, we only use type-0 vectors (scalars) of message f_{ij} denoted as $f^{(0)}_{ij}$ for attention. Note that $f^{(0)}_{ij}$ encodes directional information, as they are generated by tensor products of type-L vectors with $L \geq 0$. Inspired by GATv2 (Brody et al., 2022), we adopts multi-layer perceptron attention (MLPA) instead of dot product attention (DPA) used in Transformers (Vaswani et al., 2017). In contrast to dot product, MLPs are universal approximators (Hornik et al., 1989; Hornik, 1991; Cybenko, 1989) and can theoretically capture any attention patterns. Given $f^{(0)}_{ij}$, we uses one leaky ReLU layer and one linear layer for a_{ij}:

$$z_{ij} = a^{\top}\text{LeakyReLU}(f^{(0)}_{ij}) \quad \text{and} \quad a_{ij} = \text{softmax}_j(z_{ij}) = \frac{\exp(z_{ij})}{\sum_{k \in \mathcal{N}(i)} \exp(z_{ik})} \tag{4}$$

where a is a learnable vectors of the same dimension as $f^{(0)}_{ij}$ and z_{ij} is a single scalar. The output of attention is the sum of value v_{ij} multipled by corresponding a_{ij} over all neighboring nodes $j \in \mathcal{N}(i)$, where v_{ij} can be obtained by linear or non-linear transformations of f_{ij} as discussed below.

Non-Linear Message Passing. Values v_{ij} are features sent from one node to another, transformed with input-independent weights. We first split f_{ij} into $f^{(L)}_{ij}$ and $f^{(0)}_{ij}$, where the former consists of type-L vectors with $0 \leq L \leq L_{max}$ and the latter consists of scalars only. Then, we perform non-linear transformation to $f^{(L)}_{ij}$ to obtain non-linear message:

$$\mu_{ij} = \text{Gate}(f^{(L)}_{ij}) \quad \text{and} \quad v_{ij} = \text{Linear}([\mu_{ij} \otimes^{DTP}_{w} \text{SH}(\vec{r}_{ij})]) \tag{5}$$

We apply gate activation to $f^{(L)}_{ij}$ to obtain μ_{ij}. We use one DTP and a linear layer to enable interaction between non-linear type-L vectors, which is similar to how we transform x_{ij} into f_{ij}. Weights w here are input-independent. We can also use $f^{(L)}_{ij}$ directly as v_{ij} for linear messages.

Multi-Head Attention. Following Transformers (Vaswani et al., 2017), we can perform h parallel equivariant graph attention functions given f_{ij}. The h different outputs are concatenated and projected with a linear layer, resulting in the final output y_i as illustrated in Fig. 1(b). Note that parallelizing attention functions and concatenating can be implemented with "Reshape".

4.3 Overall Architecture

For completeness, we discuss other modules in Equiformer here.

Embedding. This module consists of atom embedding and edge-degree embedding. For the former, we use a linear layer to transform one-hot encoding of atom species. For the latter, as depicted in the right branch in Fig. 1(c), we first transform a constant one vector into messages encoding local geometry with two linear layers and one intermediate DTP layer and then use sum aggregation to encode degree information (Xu et al., 2019; Shi et al., 2022). The DTP layer has the same form as that in Eq. 3. We scale the aggregated features by dividing with the squared root of average degrees in training sets so that standard deviation of aggregated features would be close to 1.

Radial Basis and Radial Function. Relative distances $||\vec{r}_{ij}||$ parametrize weights in some DTP layers. To reflect subtle changes in $||\vec{r}_{ij}||$, we represent distances with radial basis like Gaussian radial basis (Schütt et al., 2017) and radial Bessel basis (Gasteiger et al., 2020b;a). We transform radial basis with a learnable radial function to generate weights for those DTP layers. The function consists of two MLPs with layer normalization and SiLU and a final linear layer.

Feed Forward Network. Similar to Transformers, we use two equivariant linear layers and an intermediate gate activation for the feed forward networks in Equiformer.

Output Head. The last feed forward network transforms features on each node into a scalar. We perform sum aggregation over all nodes to predict scalar quantities like energy. Similar to edge-degree embedding, we divide the aggregated scalars with the squared root of average numbers of atoms.

Methods	Task Units	α bohr^3	$\Delta\varepsilon$ meV	$\varepsilon_{\text{HOMO}}$ meV	$\varepsilon_{\text{LUMO}}$ meV	μ D	C_ν cal/mol K	G meV	H meV	R^2 bohr^3	U meV	U_0 meV	ZPVE meV
NMP (Gilmer et al., 2017)†		.092	69	43	38	.030	.040	19	17	.180	20	20	1.50
SchNet (Schütt et al., 2017)		.235	63	41	34	.033	.033	14	14	.073	19	14	1.70
Cormorant (Anderson et al., 2019)†		.085	61	34	38	.038	.026	20	21	.961	21	22	2.03
LieConv (Finzi et al., 2020)†		.084	49	30	25	.032	.038	22	24	.800	19	19	2.28
DimeNet++ (Gasteiger et al., 2020a)		**.044**	33	25	20	.030	.023	8	7	.331	6	6	1.21
TFN (Thomas et al., 2018)†		.223	58	40	38	.064	.101	-	-	-	-	-	-
SE(3)-Transformer (Fuchs et al., 2020)†		.142	53	35	33	.051	.054	-	-	-	-	-	-
EGNN (Satorras et al., 2021)†		.071	48	29	25	.029	.031	12	12	.106	12	11	1.55
PaiNN (Schütt et al., 2021)		.045	46	28	20	.012	.024	**7.35**	**5.98**	.066	**5.83**	**5.85**	1.28
TorchMD-NET (Thölke & Fabritiis, 2022)		.059	36	20	18	**.011**	.026	7.62	6.16	**.033**	6.38	6.15	1.84
SphereNet (Liu et al., 2022)		.046	32	23	18	.026	**.021**	8	6	.292	7	6	**1.12**
SEGNN (Brandstetter et al., 2022)†		.060	42	24	21	.023	.031	15	16	.660	13	15	1.62
EQGAT (Le et al., 2022)		.053	32	20	16	**.011**	.024	23	24	.382	25	25	2.00
Equiformer		.046	**30**	**15**	**14**	**.011**	.023	7.63	6.63	.251	6.74	6.59	1.26

Table 1: **MAE results on QM9 testing set.** † denotes using different data partitions.

Methods	Aspirin		Benzene		Ethanol		Malonaldehyde		Naphthalene		Salicylic acid		Toluene		Uracil	
	energy	forces	energy	forces	energy	forces	energy	forces	energy	forces	energy	forces	energy	forces	energy	forces
SchNet (Schütt et al., 2017)	16.0	58.5	3.5	13.4	3.5	16.9	5.6	28.6	6.9	25.2	8.7	36.9	5.2	24.7	6.1	24.3
DimeNet (Gasteiger et al., 2020b)	8.8	21.6	3.4	8.1	2.8	10.0	4.5	16.6	5.3	9.3	5.8	16.2	4.4	9.4	5.0	13.1
PaiNN (Schütt et al., 2021)	6.9	14.7	-	-	2.7	9.7	3.9	13.8	5.0	3.3	4.9	8.5	4.1	4.1	4.5	6.0
TorchMD-NET (Thölke & Fabritiis, 2022)	**5.3**	11.0	2.5	8.5	2.3	4.7	3.3	7.3	**3.7**	2.6	**4.0**	5.6	**3.2**	2.9	**4.1**	4.1
NequIP ($L_{max} = 3$) (Batzner et al., 2022)	5.7	8.0	-	-	**2.2**	3.1	3.3	5.6	4.9	**1.7**	4.6	**3.9**	4.0	**2.0**	4.5	**3.3**
Equiformer ($L_{max} = 2$)	**5.3**	7.2	**2.2**	**6.6**	**2.2**	3.1	3.3	5.8	**3.7**	2.1	4.5	4.1	3.8	2.1	4.3	**3.3**
Equiformer ($L_{max} = 3$)	**5.3**	**6.6**	2.5	8.1	**2.2**	**2.9**	**3.2**	**5.4**	4.4	2.0	4.3	**3.9**	3.7	2.1	4.3	3.4

Table 2: **MAE results on MD17 testing set.** Energy and force are in units of meV and meV/Å.

5 EXPERIMENT

We benchmark Equiformer on QM9 (Sec. 5.1), MD17 (Sec. 5.2) and OC20 (Sec. 5.3) datasets. Moreover, we conduct ablation studies (Sec. 5.4) to demonstrate that the proposed equivariant graph attention, consisting of MLP attention and non-linear message passing, improves upon typical dot product attention in Transformer as well as dot product attention in other equivariant Transformers. Additional results of including inversion can be found in Sec. D.2 and Sec. F.4.

5.1 QM9

Dataset. The QM9 dataset (Ruddigkeit et al., 2012; Ramakrishnan et al., 2014) (CC BY-NC SA 4.0 license) consists of 134k small molecules, and the goal is to predict their quantum properties. The data partition we use has 110k, 10k, and 11k molecules in training, validation and testing sets. We minimize mean absolute error (MAE) between prediction and normalized ground truth.

Training Details. Please refer to Sec. D.1 in appendix for details on architecture, hyper-parameters and training time.

Results. We summarize the comparison to previous models in Table 1. Equiformer achieves overall better results across 12 regression tasks compared to each individual model. The comparison to SEGNN, which uses irreps features as Equiformer, demonstrates the effectiveness of combining non-lienar message passing with MLP attention. Additionally, Equiformer achieves better results for most tasks when compared to other equivariant Transformers, which are SE(3)-Transformer, TorchMD-NET and EQGAT. This demonstrates a better adaption of Transformers to 3D graphs and the effectiveness of the proposed equivariant graph attention. We note that for the tasks of μ and R^2, PaiNN and TorchMD-NET use different architectures, which take into account the property of the task. In contrast, we use the same architecture for all tasks.We compare training time in Sec. D.3.

5.2 MD17

Dataset. The MD17 dataset (Chmiela et al., 2017; Schütt et al., 2017; Chmiela et al., 2018) (CC BY-NC) consists of molecular dynamics simulations of small organic molecules, and the goal is to predict their energy and forces. We use 950 and 50 different configurations for training and validation sets and the rest for the testing set. Forces are derived as the negative gradient of energy with respect to atomic positions. We minimize MAE between prediction and normalized ground truth.

Training Details. Please refer to Sec. E.1 in appendix for details on architecture, hyper-parameters and training time.

Results. We train Equiformer with $L_{max} = 2$ and 3 and summarize the results in Table 2. Equiformer achieves overall better results across 8 molecules compared to each individual model.

Methods	Energy MAE (eV) ↓					EwT (%) ↑				
	ID	OOD Ads	OOD Cat	OOD Both	Average	ID	OOD Ads	OOD Cat	OOD Both	Average
CGCNN (Xie & Grossman, 2018)	0.6149	0.9155	0.6219	0.8511	0.7509	3.40	1.93	3.10	2.00	2.61
SchNet (Schütt et al., 2017)	0.6387	0.7342	0.6616	0.7037	0.6846	2.96	2.33	2.94	2.21	2.61
DimeNet++ (Gasteiger et al., 2020a)	0.5621	0.7252	0.5756	0.6613	0.6311	4.25	2.07	4.10	2.41	3.21
PaiNN (Schütt et al., 2021)	0.575	0.783	0.604	0.743	0.6763	3.46	1.97	3.46	2.28	2.79
SpinConv (Shuaibi et al., 2021)	0.5583	0.7230	0.5687	0.6738	0.6310	4.08	2.26	3.82	2.33	3.12
SphereNet (Liu et al., 2022)	0.5625	0.7033	0.5708	0.6378	0.6186	4.47	2.29	4.09	2.41	3.32
SEGNN (Brandstetter et al., 2022)	0.5327	0.6921	0.5369	0.6790	0.6101	**5.37**	**2.46**	**4.91**	2.63	**3.84**
Equiformer	**0.5037**	**0.6881**	**0.5213**	**0.6301**	**0.5858**	5.14	2.41	4.67	**2.69**	3.73

Table 3: **Results on OC20 IS2RE testing set.**

Methods	Energy MAE (eV) ↓					EwT (%) ↑				
	ID	OOD Ads	OOD Cat	OOD Both	Average	ID	OOD Ads	OOD Cat	OOD Both	Average
GNS (Godwin et al., 2022)	0.54	0.65	0.55	0.59	0.5825	-	-	-	-	-
GNS + Noisy Nodes (Godwin et al., 2022)	0.47	0.51	0.48	0.46	0.4800	-	-	-	-	-
Graphormer (Shi et al., 2022)	0.4329	0.5850	0.4441	0.5299	0.4980	-	-	-	-	-
Equiformer	0.4222	0.5420	0.4231	0.4754	0.4657	7.23	3.77	7.13	4.10	5.56
Equiformer + Noisy Nodes	**0.4156**	**0.4976**	**0.4165**	**0.4344**	**0.4410**	**7.47**	**4.64**	**7.19**	**4.84**	**6.04**

Table 4: **Results on OC20 IS2RE validation set when IS2RS is adopted during training.**

Methods	Energy MAE (eV) ↓					EwT (%) ↑					Training time
	ID	OOD Ads	OOD Cat	OOD Both	Average	ID	OOD Ads	OOD Cat	OOD Both	Average	(GPU-days)
GNS + Noisy Nodes (Godwin et al., 2022)	0.4219	0.5678	0.4366	**0.4651**	0.4728	**9.12**	**4.25**	8.01	**4.64**	**6.5**	56 (TPU)
Graphormer (Shi et al., 2022)†	**0.3976**	0.5719	**0.4166**	0.5029	0.4722	8.97	3.45	**8.18**	3.79	6.1	372 (A100)
Equiformer + Noisy Nodes	0.4171	**0.5479**	0.4248	0.4741	**0.4660**	7.71	3.70	7.15	4.07	5.66	**24** (A6000)

Table 5: **Results on OC20 IS2RE testing set when IS2RS is adopted during training.** † denotes using ensemble of models trained on both IS2RE training and validation sets. In contrast, we use the same single Equiformer model in Table 4, which is trained only on the training set. Note that Equiformer achieves better results with much less computation.

Compared to TorchMD-NET, which is also an equivariant Transformer, the difference lies in the proposed equivariant graph attention, which is more expressive and can support vectors of higher degree L (i.e., we use $L_{max} = 2$ and 3) instead of restricting to type-0 and type-1 vectors (i.e., $L_{max} = 1$). For the last three molecules, although Equiformer with $L_{max} = 2$ achieves lower force MAE but higher energy MAE, we can adjust the weights of energy loss and force loss so that Equiformer achieves lower MAE for both energy and forces as shown in Table 12 in appendix. Compared to NequIP, which also uses irreps features and $L_{max} = 3$, Equiformer with $L_{max} = 2$ achieves overall lower MAE although including higher L_{max} can improve performance. When using $L_{max} = 3$, Equiformer achieves lower MAE results for most molecules. This suggests that the proposed attention can improve upon linear messages even when the size of training sets becomes small. We compare the training time of NequIP and Equiformer in Sec. E.3. Additionally, for Equiformer, increasing L_{max} from 2 to 3 improves MAE for most molecules except benzene, which results from overfitting.

5.3 OC20

Dataset. The Open Catalyst 2020 (OC20) dataset (Chanussot* et al., 2021) (Creative Commons Attribution 4.0 License) consists of larger atomic systems, each composed of a molecule called adsorbate placed on a slab called catalyst. Each input contains more atoms and more diverse atom types than QM9 and MD17. We focus on the task of initial structure to relaxed energy (IS2RE), which is to predict the energy of a relaxed structure (RS) given its initial structure (IS). Performance is measured in MAE and energy within threshold (EwT), the percentage in which predicted energy is within 0.02 eV of ground truth energy. In validation and testing sets, there are four sub-splits containing in-distribution adsorbates and catalysts (ID), out-of-distribution adsorbates (OOD-Ads), out-of-distribution catalysts (OOD-Cat), and out-of-distribution adsorbates and catalysts (OOD-Both). Please refer to Sec. F.1 for the detailed description of OC20 dataset.

Setting. We consider two training settings based on whether a node-level auxiliary task (Godwin et al., 2022) is adopted. In the first setting, we minimize MAE between predicted energy and ground truth energy without any node-level auxiliary task. In the second setting, we incorporate the task of initial structure to relaxed structure (IS2RS) as a node-level auxiliary task.

Training Details. Please refer to Sec. F.2 in appendix for details on Equiformer architecture, hyper-parameters and training time.

IS2RE Results without Node-Level Auxiliary Task. We summarize the results on validation and testing sets under the first setting in Table 15 in appendix and Table 3. Compared with state-of-the-

Index	Methods: Non-linear message passing	Methods: MLP attention	Methods: Dot product attention	Task Unit	α bohr^3	$\Delta\varepsilon$ meV	$\varepsilon_{\text{HOMO}}$ meV	$\varepsilon_{\text{LUMO}}$ meV	μ D	C_{ν} cal/mol K	Training time (minutes/epoch)	Number of parameters
1	✓	✓			.046	30	15	14	.011	.023	12.1	3.53M
2		✓			.051	32	16	16	.013	.025	7.2	3.01M
3			✓		.053	32	17	16	.013	.025	7.8	3.35M

Table 6: **Ablation study results on QM9.**

Index	Methods: Non-linear message passing	Methods: MLP attention	Methods: Dot product attention	Energy MAE (eV) ↓ ID	Energy MAE (eV) ↓ OOD Ads	Energy MAE (eV) ↓ OOD Cat	Energy MAE (eV) ↓ OOD Both	Energy MAE (eV) ↓ Average	EwT (%) ↑ ID	EwT (%) ↑ OOD Ads	EwT (%) ↑ OOD Cat	EwT (%) ↑ OOD Both	EwT (%) ↑ Average	Training time (minutes/epoch)	Number of parameters
1	✓	✓		0.5088	0.6271	0.5051	0.5545	0.5489	4.88	2.93	4.92	2.98	3.93	130.8	9.12M
2		✓		0.5168	0.6308	0.5088	0.5657	0.5555	4.59	2.82	4.79	3.02	3.81	91.2	7.84M
3			✓	0.5386	0.6382	0.5297	0.5692	0.5689	4.37	2.60	4.36	2.86	3.55	99.3	8.72M

Table 7: **Ablation study results on OC20 IS2RE validation set.**

art models like SEGNN and SphereNet, Equiformer consistently achieves the lowest MAE for all the four sub-splits in validation and testing sets. Note that EwT considers only the percentage of predictions close enough to ground truth and the distribution of errors, and therefore improvement in average errors (MAE) would not necessarily reflect that in error distributions (EwT). A more detailed discussion can be found in Sec. F.6 in appendix. We also note that models are trained by minimizing MAE, and therefore comparing MAE could mitigate the discrepancy between training objectives and evaluation metrics and that OC20 leaderboard ranks the relative performance according to MAE. Additionally, we compare the training time of SEGNN and Equiformer in Sec. F.5.

IS2RE Results with IS2RS Node-Level Auxiliary Task. We report the results on validation and testing sets in Table 4 and Table 5. As of the date of the submission of this work, Equiformer achieves the best results on IS2RE task when only IS2RE and IS2RS data are used. Notably, the result in Table 5 is achieved with much less computation. We note that under this setting, greater depths and thus more computation translate to better performance (Godwin et al., 2022) and that Equiformer demonstrates incorporating equivariant features and the proposed equivariant graph attention can improve training efficiency by $2.3\times$ to $15.5\times$ compared to invariant message passing networks and invariant Transformers.

5.4 Ablation Study

We conduct ablation studies on improvement brought by MLP attention and non-linear messages in the proposed equivariant graph attention. We modify dot product (DP) attention (Vaswani et al., 2017; Fuchs et al., 2020) so that it only differs from MLP attention in how attention weights a_{ij} are generated from f_{ij}. Please refer to Sec. C.3 in appendix for further details. For experiments on QM9 and OC20, unless otherwise stated, we follow the hyper-parameters used in previous experiments.

Result on QM9. The comparison is summarized in Table 6. Non-linear messages improve upon linear messages when MLP attention is used while non-linear messages increase the number of tensor product operations in each block from 1 to 2 and thus inevitably increase training time. On the other hand, MLP attention achieves similar results to DP attention. We conjecture that DP attention with linear operations is expressive enough to capture common attention patterns as the numbers of nighboring nodes and atom species are much smaller than those in OC20. However, MLP attention is roughly 8% faster as it directly generates scalar features and attention weights from f_{ij} instead of producing additional key and query irreps features for attention weights.

Result on OC20. We consider the setting of training without auxiliary task and summarize the comparison in Table 7. Non-linear messages consistently improve upon linear messages. In contrast to the results on QM9, MLP attention achieves better performance than DP attention and is 8% faster. We surmise this is because OC20 contains larger atomistic graphs with more diverse atom species and therefore requires more expressive attention mechanisms. Note that Equiformer can potentially improve upon previous equivariant Transformers (Fuchs et al., 2020; Thölke & Fabritiis, 2022; Le et al., 2022) since they use less expressive attention mechanisms similar to Index 3 in Table 7.

6 Conclusion

In this work, we propose Equiformer, a graph neural network (GNN) combining the strengths of Transformers and equivariant features based on irreducible representations (irreps). With irreps features, we build upon existing generic GNNs and Transformer networks by incorporating equivariant operations like tensor products. We further propose equivariant graph attention, which incorporates multi-layer perceptron attention and non-linear messages. Experiments on QM9, MD17 and OC20 demonstrate the effectiveness of Equiformer and ablation studies show the improvement of the proposed equivariant graph attention over typical attention in Transformers.

7 ETHICS STATEMENT

Equiformer achieves more accurate approximations of quantum properties calculation. We believe there is much more to be gained by harnessing these abilities for productive investigation of molecules and materials relevant to application such as energy, electronics, and pharmaceuticals, than to be lost by applying these methods for adversarial purposes like creating hazardous chemicals. Additionally, there are still substantial hurdles to go from the identification of a useful or harmful molecule to its large-scale deployment.

Moreover, we discuss several limitations of Equiformer and the proposed equivariant graph attention in Sec. G in appendix.

8 REPRODUCIBILITY STATEMENT

We include details on architectures, hyper-parameters and training time in Sec. D.1 (QM9), Sec. E.1 (MD17) and Sec. F.2 (OC20).

We submit our code reproducing the result of Equiformer on the task of α of QM9 dataset. Following the author guide, we will make a comment directed to the reviewers and area chairs and put a link to an anonymous repository.

REFERENCES

Brandon Anderson, Truong-Son Hy, and Risi Kondor. Cormorant: Covariant molecular neural networks. In *Conference on Neural Information Processing (NeurIPS)*, 2019.

Jimmy Lei Ba, Jamie Ryan Kiros, and Geoffrey E. Hinton. Layer normalization. *arxiv preprint arxiv:1607.06450*, 2016.

Alexei Baevski, Yuhao Zhou, Abdelrahman Mohamed, and Michael Auli. wav2vec 2.0: A framework for self-supervised learning of speech representations. In *Conference on Neural Information Processing (NeurIPS)*, 2020.

Simon Batzner, Albert Musaelian, Lixin Sun, Mario Geiger, Jonathan P. Mailoa, Mordechai Kornbluth, Nicola Molinari, Tess E. Smidt, and Boris Kozinsky. E(3)-equivariant graph neural networks for data-efficient and accurate interatomic potentials. *Nature Communications*, 13 (1), May 2022. doi: 10.1038/s41467-022-29939-5. URL https://doi.org/10.1038/s41467-022-29939-5.

Johannes Brandstetter, Rob Hesselink, Elise van der Pol, Erik J Bekkers, and Max Welling. Geometric and physical quantities improve e(3) equivariant message passing. In *International Conference on Learning Representations (ICLR)*, 2022. URL https://openreview.net/forum?id=_xwr8gOBeV1.

Shaked Brody, Uri Alon, and Eran Yahav. How attentive are graph attention networks? In *International Conference on Learning Representations (ICLR)*, 2022. URL https://openreview.net/forum?id=F72ximsx7C1.

Tom Brown, Benjamin Mann, Nick Ryder, Melanie Subbiah, Jared D Kaplan, Prafulla Dhariwal, Arvind Neelakantan, Pranav Shyam, Girish Sastry, Amanda Askell, Sandhini Agarwal, Ariel Herbert-Voss, Gretchen Krueger, Tom Henighan, Rewon Child, Aditya Ramesh, Daniel Ziegler, Jeffrey Wu, Clemens Winter, Chris Hesse, Mark Chen, Eric Sigler, Mateusz Litwin, Scott Gray, Benjamin Chess, Jack Clark, Christopher Berner, Sam McCandlish, Alec Radford, Ilya Sutskever, and Dario Amodei. Language models are few-shot learners. In *Conference on Neural Information Processing (NeurIPS)*, 2020.

Dan Busbridge, Dane Sherburn, Pietro Cavallo, and Nils Y. Hammerla. Relational graph attention networks. *arxiv preprint arxiv:1904.05811*, 2019.

Nicolas Carion, Francisco Massa, Gabriel Synnaeve, Nicolas Usunier, Alexander Kirillov, and Sergey Zagoruyko. End-to-end object detection with transformers. In *European Conference on Computer Vision (ECCV)*, 2020.

Lowik Chanussot*, Abhishek Das*, Siddharth Goyal*, Thibaut Lavril*, Muhammed Shuaibi*, Morgane Riviere, Kevin Tran, Javier Heras-Domingo, Caleb Ho, Weihua Hu, Aini Palizhati, Anuroop Sriram, Brandon Wood, Junwoong Yoon, Devi Parikh, C. Lawrence Zitnick, and Zachary Ulissi. Open catalyst 2020 (oc20) dataset and community challenges. *ACS Catalysis*, 2021. doi: 10.1021/acscatal.0c04525.

Zhengdao Chen, Lisha Li, and Joan Bruna. Supervised community detection with line graph neural networks. In *International Conference on Learning Representations (ICLR)*, 2019. URL https://openreview.net/forum?id=H1g0Z3A9Fm.

Stefan Chmiela, Alexandre Tkatchenko, Huziel E. Sauceda, Igor Poltavsky, Kristof T. Schütt, and Klaus-Robert Müller. Machine learning of accurate energy-conserving molecular force fields. *Science Advances*, 3(5):e1603015, 2017. doi: 10.1126/sciadv.1603015. URL https://www.science.org/doi/abs/10.1126/sciadv.1603015.

Stefan Chmiela, Huziel E. Sauceda, Klaus-Robert Müller, and Alexandre Tkatchenko. Towards exact molecular dynamics simulations with machine-learned force fields. *Nature Communications*, 9(1), sep 2018. doi: 10.1038/s41467-018-06169-2.

Taco Cohen and Max Welling. Group equivariant convolutional networks. In *International Conference on Machine Learning (ICML)*, 2016.

Taco S. Cohen, Mario Geiger, Jonas Köhler, and Max Welling. Spherical CNNs. In *International Conference on Learning Representations (ICLR)*, 2018. URL https://openreview.net/forum?id=Hkbd5xZRb.

George V. Cybenko. Approximation by superpositions of a sigmoidal function. *Mathematics of Control, Signals and Systems*, 2:303–314, 1989.

Jacob Devlin, Ming-Wei Chang, Kenton Lee, and Kristina Toutanova. Bert: Pre-training of deep bidirectional transformers for language understanding. *arxiv preprint arxiv:1810.04805*, 2019.

Alexey Dosovitskiy, Lucas Beyer, Alexander Kolesnikov, Dirk Weissenborn, Xiaohua Zhai, Thomas Unterthiner, Mostafa Dehghani, Matthias Minderer, Georg Heigold, Sylvain Gelly, Jakob Uszkoreit, and Neil Houlsby. An image is worth 16x16 words: Transformers for image recognition at scale. In *International Conference on Learning Representations (ICLR)*, 2021. URL https://openreview.net/forum?id=YicbFdNTTy.

Mildred S Dresselhaus, Gene Dresselhaus, and Ado Jorio. *Group theory*. Springer, Berlin, Germany, 2008 edition, March 2007.

Vijay Prakash Dwivedi and Xavier Bresson. A generalization of transformer networks to graphs. 2020.

Stefan Elfwing, Eiji Uchibe, and Kenji Doya. Sigmoid-weighted linear units for neural network function approximation in reinforcement learning. *arXiv preprint arXiv:1702.03118*, 2017.

Marc Finzi, Samuel Stanton, Pavel Izmailov, and Andrew Gordon Wilson. Generalizing convolutional neural networks for equivariance to lie groups on arbitrary continuous data. *arXiv preprint arXiv:2002.12880*, 2020.

Nathan Frey, Ryan Soklaski, Simon Axelrod, Siddharth Samsi, Rafael Gomez-Bombarelli, Connor Coley, and Vijay Gadepally. Neural scaling of deep chemical models. *ChemRxiv*, 2022. doi: 10.26434/chemrxiv-2022-3s512.

Fabian Fuchs, Daniel E. Worrall, Volker Fischer, and Max Welling. Se(3)-transformers: 3d roto-translation equivariant attention networks. In *Conference on Neural Information Processing (NeurIPS)*, 2020.

Hongyang Gao and Shuiwang Ji. Graph representation learning via hard and channel-wise attention networks. *Proceedings of the 25th ACM SIGKDD International Conference on Knowledge Discovery & Data Mining*, 2019.

Johannes Gasteiger, Shankari Giri, Johannes T. Margraf, and Stephan Günnemann. Fast and uncertainty-aware directional message passing for non-equilibrium molecules. In *Machine Learning for Molecules Workshop, NeurIPS*, 2020a.

Johannes Gasteiger, Janek Groß, and Stephan Günnemann. Directional message passing for molecular graphs. In *International Conference on Learning Representations (ICLR)*, 2020b.

Johannes Gasteiger, Muhammed Shuaibi, Anuroop Sriram, Stephan Günnemann, Zachary Ulissi, C. Lawrence Zitnick, and Abhishek Das. How do graph networks generalize to large and diverse molecular systems? *arxiv preprint arxiv:2204.02782*, 2022.

Mario Geiger, Tess Smidt, Alby M., Benjamin Kurt Miller, Wouter Boomsma, Bradley Dice, Kostiantyn Lapchevskyi, Maurice Weiler, Michał Tyszkiewicz, Simon Batzner, Dylan Madisetti, Martin Uhrin, Jes Frellsen, Nuri Jung, Sophia Sanborn, Mingjian Wen, Josh Rackers, Marcel Rød, and Michael Bailey. e3nn/e3nn: 2022-04-13, April 2022. URL https://doi.org/10.5281/zenodo.6459381.

Justin Gilmer, Samuel S. Schoenholz, Patrick F. Riley, Oriol Vinyals, and George E. Dahl. Neural message passing for quantum chemistry. In *International Conference on Machine Learning (ICML)*, 2017.

Jonathan Godwin, Michael Schaarschmidt, Alexander L Gaunt, Alvaro Sanchez-Gonzalez, Yulia Rubanova, Petar Veličković, James Kirkpatrick, and Peter Battaglia. Simple GNN regularisation for 3d molecular property prediction and beyond. In *International Conference on Learning Representations (ICLR)*, 2022. URL https://openreview.net/forum?id=1wVvweK3oIb.

William L. Hamilton, Rex Ying, and Jure Leskovec. Inductive representation learning on large graphs. In *Conference on Neural Information Processing (NeurIPS)*, 2017.

Kurt Hornik. Approximation capabilities of multilayer feedforward networks. *Neural Networks*, 4(2):251–257, 1991. ISSN 0893-6080. doi: https://doi.org/10.1016/0893-6080(91)90009-T. URL https://www.sciencedirect.com/science/article/pii/089360809190009T.

Kurt Hornik, Maxwell Stinchcombe, and Halbert White. Multilayer feedforward networks are universal approximators. *Neural Networks*, 2(5):359–366, 1989. ISSN 0893-6080. doi: https://doi.org/10.1016/0893-6080(89)90020-8. URL https://www.sciencedirect.com/science/article/pii/0893608089900208.

Andrew G. Howard, Menglong Zhu, Bo Chen, Dmitry Kalenichenko, Weijun Wang, Tobias Weyand, Marco Andreetto, and Hartwig Adam. Mobilenets: Efficient convolutional neural networks for mobile vision applications. *ArXiv*, abs/1704.04861, 2017.

Weihua Hu, Matthias Fey, Marinka Zitnik, Yuxiao Dong, Hongyu Ren, Bowen Liu, Michele Catasta, and Jure Leskovec. Open graph benchmark: Datasets for machine learning on graphs. *arXiv preprint arXiv:2005.00687*, 2020.

Weihua Hu, Matthias Fey, Hongyu Ren, Maho Nakata, Yuxiao Dong, and Jure Leskovec. Ogb-lsc: A large-scale challenge for machine learning on graphs. *arXiv preprint arXiv:2103.09430*, 2021.

Weile Jia, Han Wang, Mohan Chen, Denghui Lu, Lin Lin, Roberto Car, Weinan E, and Linfeng Zhang. Pushing the limit of molecular dynamics with ab initio accuracy to 100 million atoms with machine learning. In *Proceedings of the International Conference for High Performance Computing, Networking, Storage and Analysis*, SC '20. IEEE Press, 2020.

Bowen Jing, Stephan Eismann, Patricia Suriana, Raphael John Lamarre Townshend, and Ron Dror. Learning from protein structure with geometric vector perceptrons. In *International Conference on Learning Representations (ICLR)*, 2021. URL https://openreview.net/forum?id=1YLJDvSx6J4.

Salman Khan, Muzammal Naseer, Munawar Hayat, Syed Waqas Zamir, Fahad Shahbaz Khan, and Mubarak Shah. Transformers in vision: A survey. 2021.

Dongkwan Kim and Alice Oh. How to find your friendly neighborhood: Graph attention design with self-supervision. In *International Conference on Learning Representations (ICLR)*, 2021. URL https://openreview.net/forum?id=Wi5KUNlqWty.

Thomas N. Kipf and Max Welling. Semi-supervised classification with graph convolutional networks. In *International Conference on Learning Representations (ICLR)*, 2017.

Johannes Klicpera, Florian Becker, and Stephan Günnemann. Gemnet: Universal directional graph neural networks for molecules. In *Conference on Neural Information Processing (NeurIPS)*, 2021.

Risi Kondor, Zhen Lin, and Shubhendu Trivedi. Clebsch–gordan nets: a fully fourier space spherical convolutional neural network. In *Advances in Neural Information Processing Systems 32*, pp. 10117–10126, 2018.

Devin Kreuzer, Dominique Beaini, William L. Hamilton, Vincent Létourneau, and Prudencio Tossou. Rethinking graph transformers with spectral attention. In *Conference on Neural Information Processing (NeurIPS)*, 2021. URL https://openreview.net/forum?id=huAdB-Tj4yG.

Tuan Le, Frank Noé, and Djork-Arné Clevert. Equivariant graph attention networks for molecular property prediction. *arXiv preprint arXiv:2202.09891*, 2022.

Yi Liu, Limei Wang, Meng Liu, Yuchao Lin, Xuan Zhang, Bora Oztekin, and Shuiwang Ji. Spherical message passing for 3d molecular graphs. In *International Conference on Learning Representations (ICLR)*, 2022. URL https://openreview.net/forum?id=givsRXsOt9r.

Denghui Lu, Han Wang, Mohan Chen, Lin Lin, Roberto Car, Weinan E, Weile Jia, and Linfeng Zhang. 86 pflops deep potential molecular dynamics simulation of 100 million atoms with ab initio accuracy. *Computer Physics Communications*, 259:107624, 2021. ISSN 0010-4655. doi: https://doi.org/10.1016/j.cpc.2020.107624. URL https://www.sciencedirect.com/science/article/pii/S001046552030299X.

Benjamin Kurt Miller, Mario Geiger, Tess E. Smidt, and Frank Noé. Relevance of rotationally equivariant convolutions for predicting molecular properties. *arxiv preprint arxiv:2008.08461*, 2020.

Albert Musaelian, Simon Batzner, Anders Johansson, Lixin Sun, Cameron J. Owen, Mordechai Kornbluth, and Boris Kozinsky. Learning local equivariant representations for large-scale atomistic dynamics. *arxiv preprint arxiv:2204.05249*, 2022.

Adam Paszke, Sam Gross, Francisco Massa, Adam Lerer, James Bradbury, Gregory Chanan, Trevor Killeen, Zeming Lin, Natalia Gimelshein, Luca Antiga, Alban Desmaison, Andreas Kopf, Edward Yang, Zachary DeVito, Martin Raison, Alykhan Tejani, Sasank Chilamkurthy, Benoit Steiner, Lu Fang, Junjie Bai, and Soumith Chintala. Pytorch: An imperative style, high-performance deep learning library. In H. Wallach, H. Larochelle, A. Beygelzimer, F. d'Alché-Buc, E. Fox, and R. Garnett (eds.), *Advances in Neural Information Processing Systems 32*, pp. 8024–8035. Curran Associates, Inc., 2019. URL http://papers.neurips.cc/paper/9015-pytorch-an-imperative-style-high-performance-deep-learning-library.pdf.

Zhuoran Qiao, Matthew Welborn, Animashree Anandkumar, Frederick R. Manby, and Thomas F. Miller. OrbNet: Deep learning for quantum chemistry using symmetry-adapted atomic-orbital features. *The Journal of Chemical Physics*, 153(12):124111, sep 2020. doi: 10.1063/5.0021955. URL https://doi.org/10.1063%2F5.0021955.

Joshua A. Rackers, Lucas Tecot, Mario Geiger, and Tess E. Smidt. Cracking the quantum scaling limit with machine learned electron densities. *arxiv preprint arxiv:2201.03726*, 2022.

Prajit Ramachandran, Barret Zoph, and Quoc V. Le. Searching for activation functions. *arXiv preprint arXiv:1710.05941*, 2017.

Raghunathan Ramakrishnan, Pavlo O Dral, Matthias Rupp, and O Anatole von Lilienfeld. Quantum chemistry structures and properties of 134 kilo molecules. *Scientific Data*, 1, 2014.

Bharath Ramsundar, Peter Eastman, Patrick Walters, Vijay Pande, Karl Leswing, and Zhenqin Wu. *Deep Learning for the Life Sciences*. O'Reilly Media, 2019. https://www.amazon.com/Deep-Learning-Life-Sciences-Microscopy/dp/1492039837.

Yu Rong, Yatao Bian, Tingyang Xu, Weiyang Xie, Ying WEI, Wenbing Huang, and Junzhou Huang. Self-supervised graph transformer on large-scale molecular data. In *Conference on Neural Information Processing (NeurIPS)*, 2020.

Lars Ruddigkeit, Ruud van Deursen, Lorenz C. Blum, and Jean-Louis Reymond. Enumeration of 166 billion organic small molecules in the chemical universe database gdb-17. *Journal of Chemical Information and Modeling*, 52(11):2864–2875, 2012. doi: 10.1021/ci300415d. URL https://doi.org/10.1021/ci300415d. PMID: 23088335.

Olga Russakovsky, Jia Deng, Hao Su, Jonathan Krause, Sanjeev Satheesh, Sean Ma, Zhiheng Huang, Andrej Karpathy, Aditya Khosla, Michael Bernstein, Alexander C. Berg, and Li Fei-Fei. ImageNet Large Scale Visual Recognition Challenge. *International Journal of Computer Vision (IJCV)*, 115 (3):211–252, 2015. doi: 10.1007/s11263-015-0816-y.

Alvaro Sanchez-Gonzalez, Jonathan Godwin, Tobias Pfaff, Rex Ying, Jure Leskovec, and Peter W. Battaglia. Learning to simulate complex physics with graph networks. In *International Conference on Machine Learning (ICML)*, 2020.

Víctor Garcia Satorras, Emiel Hoogeboom, and Max Welling. E(n) equivariant graph neural networks. In *International Conference on Machine Learning (ICML)*, 2021.

K. T. Schütt, P.-J. Kindermans, H. E. Sauceda, S. Chmiela, A. Tkatchenko, and K.-R. Müller. Schnet: A continuous-filter convolutional neural network for modeling quantum interactions. In *Conference on Neural Information Processing (NeurIPS)*, 2017.

Kristof T. Schütt, Farhad Arbabzadah, Stefan Chmiela, Klaus R. Müller, and Alexandre Tkatchenko. Quantum-chemical insights from deep tensor neural networks. *Nature Communications*, 8(1), jan 2017. doi: 10.1038/ncomms13890.

Kristof T. Schütt, Oliver T. Unke, and Michael Gastegger. Equivariant message passing for the prediction of tensorial properties and molecular spectra. In *International Conference on Machine Learning (ICML)*, 2021.

Yu Shi, Shuxin Zheng, Guolin Ke, Yifei Shen, Jiacheng You, Jiyan He, Shengjie Luo, Chang Liu, Di He, and Tie-Yan Liu. Benchmarking graphormer on large-scale molecular modeling datasets. *arxiv preprint arxiv:2203.04810*, 2022.

Yunsheng Shi, Zhengjie Huang, Shikun Feng, Hui Zhong, Wenjin Wang, and Yu Sun. Masked label prediction: Unified message passing model for semi-supervised classification. *arxiv preprint arxiv:2009.03509*, 2020.

Muhammed Shuaibi, Adeesh Kolluru, Abhishek Das, Aditya Grover, Anuroop Sriram, Zachary Ulissi, and C. Lawrence Zitnick. Rotation invariant graph neural networks using spin convolutions. *arxiv preprint arxiv:2106.09575*, 2021.

Tess E. Smidt, Mario Geiger, and Benjamin Kurt Miller. Finding symmetry breaking order parameters with euclidean neural networks. *Physical Review Research*, 3(1), jan 2021. doi: 10.1103/physrevresearch.3.l012002. URL https://doi.org/10.1103%2Fphysrevresearch.3.l012002.

Anuroop Sriram, Abhishek Das, Brandon M Wood, and C. Lawrence Zitnick. Towards training billion parameter graph neural networks for atomic simulations. In *International Conference on Learning Representations*, 2022. URL https://openreview.net/forum?id=0jP2n0YFmKG.

Nitish Srivastava, Geoffrey Hinton, Alex Krizhevsky, Ilya Sutskever, and Ruslan Salakhutdinov. Dropout: A simple way to prevent neural networks from overfitting. *Journal of Machine Learning Research*, 15(56):1929–1958, 2014. URL http://jmlr.org/papers/v15/srivastava14a.html.

Philipp Thölke and Gianni De Fabritiis. Equivariant transformers for neural network based molecular potentials. In *International Conference on Learning Representations (ICLR)*, 2022. URL https://openreview.net/forum?id=zNHzqZ9wrRB.

Nathaniel Thomas, Tess E. Smidt, Steven Kearnes, Lusann Yang, Li Li, Kai Kohlhoff, and Patrick Riley. Tensor field networks: Rotation- and translation-equivariant neural networks for 3d point clouds. *arxiv preprint arXiv:1802.08219*, 2018.

Hugo Touvron, Matthieu Cord, Matthijs Douze, Francisco Massa, Alexandre Sablayrolles, and Hervé Jégou. Training data-efficient image transformers & distillation through attention. *arXiv preprint arXiv:2012.12877*, 2020.

Raphael J. L. Townshend, Brent Townshend, Stephan Eismann, and Ron O. Dror. Geometric prediction: Moving beyond scalars. *arXiv preprint arXiv:2006.14163*, 2020.

Raphael John Lamarre Townshend, Martin Vögele, Patricia Adriana Suriana, Alexander Derry, Alexander Powers, Yianni Laloudakis, Sidhika Balachandar, Bowen Jing, Brandon M. Anderson, Stephan Eismann, Risi Kondor, Russ Altman, and Ron O. Dror. ATOM3d: Tasks on molecules in three dimensions. In *Thirty-fifth Conference on Neural Information Processing Systems Datasets and Benchmarks Track (Round 1)*, 2021. URL https://openreview.net/forum?id=FkDZLpK1Ml2.

Oliver T. Unke and Markus Meuwly. PhysNet: A neural network for predicting energies, forces, dipole moments, and partial charges. *Journal of Chemical Theory and Computation*, 15(6): 3678–3693, may 2019.

Oliver Thorsten Unke, Mihail Bogojeski, Michael Gastegger, Mario Geiger, Tess Smidt, and Klaus Robert Muller. SE(3)-equivariant prediction of molecular wavefunctions and electronic densities. In A. Beygelzimer, Y. Dauphin, P. Liang, and J. Wortman Vaughan (eds.), *Conference on Neural Information Processing (NeurIPS)*, 2021. URL https://openreview.net/forum?id=auGY2UQfhSu.

Ashish Vaswani, Noam Shazeer, Niki Parmar, Jakob Uszkoreit, Llion Jones, Aidan N. Gomez, Lukasz Kaiser, and Illia Polosukhin. Attention is all you need. In *Conference on Neural Information Processing (NeurIPS)*, 2017.

Petar Veličković, Guillem Cucurull, Arantxa Casanova, Adriana Romero, Pietro Liò, and Yoshua Bengio. Graph attention networks. In *International Conference on Learning Representations (ICLR)*, 2018. URL https://openreview.net/forum?id=rJXMpikCZ.

Maurice Weiler, Mario Geiger, Max Welling, Wouter Boomsma, and Taco Cohen. 3D Steerable CNNs: Learning Rotationally Equivariant Features in Volumetric Data. In *Advances in Neural Information Processing Systems 32*, pp. 10402–10413, 2018.

Daniel E. Worrall, Stephan J. Garbin, Daniyar Turmukhambetov, and Gabriel J. Brostow. Harmonic networks: Deep translation and rotation equivariance. *arxiv preprint arxiv:1612.04642*, 2016.

Tian Xie and Jeffrey C. Grossman. Crystal graph convolutional neural networks for an accurate and interpretable prediction of material properties. *Physical Review Letters*, 120(14), apr 2018. doi: 10.1103/physrevlett.120.145301. URL https://doi.org/10.1103%2Fphysrevlett.120.145301.

Keyulu Xu, Weihua Hu, Jure Leskovec, and Stefanie Jegelka. How powerful are graph neural networks? In *International Conference on Learning Representations (ICLR)*, 2019. URL https://openreview.net/forum?id=ryGs6iA5Km.

Chengxuan Ying, Tianle Cai, Shengjie Luo, Shuxin Zheng, Guolin Ke, Di He, Yanming Shen, and Tie-Yan Liu. Do transformers really perform badly for graph representation? In *Conference on Neural Information Processing (NeurIPS)*, 2021. URL https://openreview.net/forum?id=OeWooOxFwDa.

A. Zee. *Group Theory in a Nutshell for Physicists*. Princeton University Press, USA, 2016.

Jiani Zhang, Xingjian Shi, Junyuan Xie, Hao Ma, Irwin King, and Dit-Yan Yeung. Gaan: Gated attention networks for learning on large and spatiotemporal graphs. In *Proceedings of the Thirty-Fourth Conference on Uncertainty in Artificial Intelligence*, pp. 339–349, 2018a.

Linfeng Zhang, Jiequn Han, Han Wang, Roberto Car, and Weinan E. Deep potential molecular dynamics: A scalable model with the accuracy of quantum mechanics. *Phys. Rev. Lett.*, 120: 143001, Apr 2018b. doi: 10.1103/PhysRevLett.120.143001. URL https://link.aps.org/doi/10.1103/PhysRevLett.120.143001.

APPENDIX

A Additional background

- A.1 Group theory
- A.2 Equivariance
- A.3 Equivariant features based on vector spaces of irreducible representations
- A.4 Tensor product

B Related works

- B.1 Graph neural networks for 3D atomistic graphs
- B.2 Invariant GNNs
- B.3 Attention and Transformer

C Details of architecture

- C.1 Equivariant operation used in Equiformer
- C.2 Equiformer architecture
- C.3 Dot product attention
- C.4 Discussion on computational complexity

D Details of experiments on QM9

- D.1 Training details
- D.2 Comparison between $SE(3)$ and $E(3)$ equivariance
- D.3 Comparison of training time and numbers of parameters

E Details of experiments on MD17

- E.1 Training details
- E.2 Additional comparison of performance to TorchMD-NET
- E.3 Comparison of training time and numbers of parameters

F Details of experiments on OC20

- F.1 Detailed description of OC20 dataset
- F.2 Training details
- F.3 Results on IS2RE validation set
- F.4 Comparison between $SE(3)$ and $E(3)$ equivariance
- F.5 Comparison of training time and numbers of parameters
- F.6 Error distributions

G Limitations

A ADDITIONAL BACKGROUND

In this section, we provide additional mathematical background helpful for the discussion of the proposed method. Other works (Thomas et al., 2018; Weiler et al., 2018; Kondor et al., 2018; Anderson et al., 2019; Fuchs et al., 2020; Brandstetter et al., 2022) also provide similar background. We encourage interested readers to see these works (Zee, 2016; Dresselhaus et al., 2007) for more in-depth and pedagogical presentations.

A.1 GROUP THEORY

Definition of Groups. A group is an algebraic structure that consists of a set G and a binary operator $\circ : G \times G \rightarrow G$ and is typically denoted as G. Groups satisfy the following four axioms:

1. Closure: $g \circ h \in G$ for all $g, h \in G$.
2. Identity: There exists an identity element $e \in G$ such that $g \circ e = e \circ g = g$ for all $g \in G$.
3. Inverse: For each $g \in G$, there exists an inverse element $g^{-1} \in G$ such that $g \circ g^{-1} = g^{-1} \circ g = e$.

4. Associativity: $f \circ g \circ h = (f \circ g) \circ h = f \circ (g \circ h)$ for all $f, g, h \in G$.

In this work, we focus on 3D rotation, translation and inversion. Relevant groups include:

1. The Euclidean group in three dimensions $E(3)$: 3D rotation, translation and inversion.
2. The special Euclidean group in three dimensions $SE(3)$: 3D rotation and translation.
3. The orthogonal group in three dimensions $O(3)$: 3D rotation and inversion.
4. The special orthogonal group in three dimensions $SO(3)$: 3D rotation.

Group Representations. The actions of groups define transformations. Formally, a transformation acting on vector space X parametrized by group element $g \in G$ is an injective function $T_g : X \to X$. A powerful result of group representation theory is that these transformations can be expressed as matrices which act on vector spaces via matrix multiplication. These matrices are called the group representations. Formally, a group representation $D : G \to GL(N)$ is a mapping between a group G and a set of $N \times N$ invertible matrices. The group representation $D(g) : X \to X$ maps an N-dimensional vector space X onto itself and satisfies $D(g)D(h) = D(g \circ h)$ for all $g, h \in G$.

How a group is represented depends on the vector space it acts on. If there exists a change of basis P in the form of an $N \times N$ matrix such that $P^{-1}D(g)P = D'(g)$ for all $g \in G$, then we say the two group representations are equivalent. If $D'(g)$ is block diagonal, which means that g acts on independent subspaces of the vector space, the representation $D(g)$ is reducible. A particular class of representations that are convenient for composable functions are irreducible representations or "irreps", which cannot be further reduced. We can express any group representation of $SO(3)$ as a direct sum (concatentation) of irreps (Zee, 2016; Dresselhaus et al., 2007; Geiger et al., 2022):

$$D(g) = P^{-1}\left(\bigoplus_i D_{l_i}(g)\right)P = P^{-1}\begin{pmatrix} D_{l_0}(g) & & \\ & D_{l_1}(g) & \\ & & \ldots\ldots \end{pmatrix}P \tag{6}$$

where $D_{l_i}(g)$ are Wigner-D matrices with degree l_i as metnioned in Sec. 3.2.

A.2 Equivariance

Definition of Equivariance and Invariance. Equivariance is a property of a function $f : X \to Y$ mapping between vector spaces X and Y. Given a group G and group representations $D_X(g)$ and $D_Y(g)$ in input and output spaces X and Y, f is equivariant to G if $D_Y(g)f(x) = f(D_X(g)x)$ for all $x \in X$ and $g \in G$. Invariance corresponds to the case where $D_Y(g)$ is the identity I for all $g \in G$.

Equivariance in Neural Networks. Group equivariant neural networks are guaranteed to to make equivariant predictions on data transformed by a group. Additionally, they are found to be data-efficient and generalize better than non-symmetry-aware and invariant methods (Batzner et al., 2022; Rackers et al., 2022; Frey et al., 2022). For 3D atomistic graphs, we consider equivariance to the Euclidean group $E(3)$, which consists of 3D rotation, translation and inversion. For translation, we operate on relative positions and therefore our networks are invariant to 3D translation. We achieve equivariance to rotation and inversion by representing our input data, intermediate features and outputs in vector spaces of $O(3)$ irreps and acting on them with only equivariant operations.

A.3 Equivariant Features Based on Vector Spaces of Irreducible Representations

Irreducible Representations of Inversion. The group of inversion $\mathbb{Z}_2$ only has two elements, identity and inversion, and two irreps, even e and odd o. Vectors transformed by irrep e do not change sign under inversion while those by irrep o do. We create irreps of $O(3)$ by simply multiplying those of $SO(3)$ and $\mathbb{Z}_2$ and introduce parity p to type-L vectors to denote how they transform under inversion. Thus, type-L vectors in $SO(3)$ become type-(L, p) vectors in $O(3)$, where p is e or o.

Irreps Features. As discussed in Sec. 3.2 in the main text, we use type-L vectors for $SE(3)$-equivariant irreps features[1] and type-(L, p) vectors for $E(3)$-equivariant irreps features. Parity p

[1] In SEGNN (Brandstetter et al., 2022), they are also referred to as steerable features. We use the term "irreps features" to remain consistent with `e3nn` (Geiger et al., 2022) library.

denotes whether vectors change sign under inversion and can be either e (even) or o (odd). Vectors with $p = o$ change sign under inversion while those with $p = e$ do not. Scalar features correspond to type-0 vectors in the case of $SE(3)$-equivariance and correspond to type-$(0, e)$ in the case of $E(3)$-equivariance whereas type-$(0, o)$ vectors correspond to pseudo-scalars. Euclidean vectors in $\mathbb{R}^3$ correspond to type-1 vectors and type-$(1, o)$ vectors whereas type-$(1, e)$ vectors correspond to pseudo-vectors. Note that type-(L, e) vectors and type-(L, o) vectors are considered vectors of different types in equivariant linear layers and layer normalizations.

Spherical Harmonics. Euclidean vectors $\vec{r}$ in $\mathbb{R}^3$ can be projected into type-L vectors $f^{(L)}$ by using spherical harmonics $Y^{(L)}$: $f^{(L)} = Y^{(L)}(\frac{\vec{r}}{||\vec{r}||})$ (Smidt et al., 2021). This is equivalent to the Fourier transform of the angular degree of freedom $\frac{\vec{r}}{||\vec{r}||}$, which can be optionally weighted by $||\vec{r}||$. In the case of $SE(3)$-equivariance, $f^{(L)}$ transforms in the same manner as type-L vectors. For $E(3)$-equivariance, $f^{(L)}$ behaves as type-(L, p) vectors, where $p = e$ if L is even and $p = o$ if L is odd.

Vectors of Higher L and Other Parities. Although previously we have restricted concrete examples of vector spaces of $O(3)$ irreps to commonly encountered scalars (type-$(0, e)$ vectors) and Euclidean vectors (type-$(1, o)$ vectors), vector of higher L and other parities are equally physical. For example, the moment of inertia (how an object rotates under torque) transforms as a 3×3 symmetric matrix, which has symmetric-traceless components behaving as type-$(2, e)$ vectors. Elasticity (how an object deforms under loading) transforms as a rank-4 or $3 \times 3 \times 3 \times 3$ symmetric tensor, which includes components acting as type-$(4, e)$ vectors.

A.4 Tensor Product

Tensor Product for $O(3)$. We use tensor products to interact different type-(L, p) vectors. We extend our discussion in Sec. 3.3 in the main text to include inversion and type-(L, p) vectors. The tensor product denoted as $\otimes$ uses Clebsch-Gordan coefficients to combine type-(L_1, p_1) vector $f^{(L_1,p_1)}$ and type-(L_2, p_2) vector $g^{(L_2,p_2)}$ and produces type-(L_3, p_3) vector $h^{(L_3,p_3)}$ as follows:

$$h^{(L_3,p_3)}_{m_3} = (f^{(L_1,p_1)} \otimes g^{(L_2,p_2)})_{m_3} = \sum_{m_1=-L_1}^{L_1} \sum_{m_2=-L_2}^{L_2} C^{(L_3,m_3)}_{(L_1,m_1)(L_2,m_2)} f^{(L_1,p_1)}_{m_1} g^{(L_2,p_2)}_{m_2} \tag{7}$$

$$p_3 = p_1 \times p_2 \tag{8}$$

The only difference of tensor products for $O(3)$ as described in Eq. 7 from those for $SO(3)$ described in Eq. 1 is that we additionally keep track of the output parity p_3 as in Eq. 8 and use the following multiplication rules: $e \times e = e$, $o \times o = e$, and $e \times o = o \times e = o$. For example, the tensor product of a type-$(1, o)$ vector and a type-$(1, e)$ vector can result in one type-$(0, o)$ vector, one type-$(1, o)$ vector, and one type-$(2, o)$ vector.

Clebsch-Gordan Coefficients. The Clebsch-Gordan coefficients for $SO(3)$ are computed from integrals over the basis functions of a given irreducible representation, e.g., the real spherical harmonics, as shown below and are tabulated to avoid unnecessary computation.

$$C^{(L_3,m_3)}_{(L_1,m_1)(L_2,m_2)} = |L_1 m_1; L_2 m_2\rangle \langle L_3 m_3| = \int d\Omega Y^{(L_1)*}_{m_1}(\Omega) Y^{(L_2)*}_{m_2}(\Omega) Y^{(L_3)}_{m_3}(\Omega) \tag{9}$$

For many combinations of L_1, L_2, and L_3, the Clebsch-Gordan coefficients are zero. The gives rise to the following selection rule for non-trivial coefficients: $-|L_1 + L_2| \leq L_3 \leq |L_1 + L_2|$.

Examples of Tensor Products. Tensor products generally define the interaction between different type-(L, p) vectors in a symmetry-preserving manner and consist of common operations as follows:

1. Scalar-scalar multiplication: scalar $(L = 0, p = e) \otimes$ scalar $(L = 0, p = e) \rightarrow$ scalar $(L = 0, p = e)$.

2. Scalar-vector multiplication: scalar $(L = 0, p = e) \otimes$ vector $(L = 1, p = o) \rightarrow$ vector $(L = 1, p = o)$.
3. Vector dot product: vector $(L = 1, p = o) \otimes$ vector $(L = 1, p = o) \rightarrow$ scalar $(L = 0, p = e)$.
4. Vector cross product: vector $(L = 1, p = o) \otimes$ vector $(L = 1, p = o) \rightarrow$ pseudo-vector $(L = 1, p = e)$.

B Related Works

B.1 Graph Neural Networks for 3D Atomistic Graphs

Graph neural networks (GNNs) are well adapted to perform property prediction of atomic systems because they can handle discrete and topological structures. There are two main ways to represent atomistic graphs (Townshend et al., 2021), which are chemical bond graphs, sometimes denoted as 2D graphs, and 3D spatial graphs. Chemical bond graphs use edges to represent covalent bonds without considering 3D geometry. Due to their similarity to graph structures in other applications, generic GNNs (Hamilton et al., 2017; Gilmer et al., 2017; Kipf & Welling, 2017; Xu et al., 2019; Veličković et al., 2018; Brody et al., 2022) can be directly applied to predict their properties (Ruddigkeit et al., 2012; Ramakrishnan et al., 2014; Ramsundar et al., 2019; Hu et al., 2020; 2021). On the other hand, 3D spatial graphs consider positions of atoms in 3D spaces and therefore 3D geometry. Although 3D graphs can faithfully represent atomistic systems, one challenge of moving from chemical bond graphs to 3D spatial graphs is to remain invariant or equivariant to geometric transformation acting on atom positions. Therefore, invariant neural networks and equivariant neural networks have been proposed for 3D atomistic graphs, with the former leveraging invariant information like distances and angles and the latter operating on geometric tensors like type-L vectors.

B.2 Invariant GNNs

Previous works (Schütt et al., 2017; Xie & Grossman, 2018; Unke & Meuwly, 2019; Gasteiger et al., 2020b;a; Qiao et al., 2020; Liu et al., 2022; Shuaibi et al., 2021; Klicpera et al., 2021) extract invariant information from 3D atomistic graphs and operate on the resulting invariant graphs. They mainly differ in leveraging different geometric information such as distances, bond angles (3 atom features) or dihedral angles (4 atom features). SchNet (Schütt et al., 2017) uses relative distances and proposes continuous-filter convolutional layers to learn local interaction between atom pairs. DimeNet series (Gasteiger et al., 2020b;a) incorporate bond angles by using triplet representations of atoms. SphereNet (Liu et al., 2022) and GemNet (Klicpera et al., 2021; Gasteiger et al., 2022) further extend to consider dihedral angles for better performance. In order to consider directional information contained in angles, they rely on triplet or quadruplet representations of atoms. In addition to being memory-intensive (Sriram et al., 2022), they also change graph structures by introducing higher-order interaction terms (Chen et al., 2019), which would require non-trivial modifications to generic GNNs in order to apply them to 3D graphs. In contrast, the proposed Equiformer uses equivariant irreps features to consider directional information without complicating graph structures and therefore can directly inherit the design of generic GNNs.

B.3 Attention and Transformer

Graph Attention. Graph attention networks (GAT) (Veličković et al., 2018; Brody et al., 2022) use multi-layer perceptrons (MLP) to calculate attention weights in a similar manner to message passing networks. Subsequent works using graph attention mechanisms follow either GAT-like MLP attention (Busbridge et al., 2019; Kim & Oh, 2021) or Transformer-like dot product attention (Zhang et al., 2018a; Gao & Ji, 2019; Shi et al., 2020; Dwivedi & Bresson, 2020; Kim & Oh, 2021; Kreuzer et al., 2021). In particular, Kim *et al.* (Kim & Oh, 2021) compares these two types of attention mechanisms empirically under a self-supervised setting. Brody *et al.* (Brody et al., 2022) analyzes their theoretical differences and compares their performance in general settings.

Graph Transformer. A different line of research focuses on adapting standard Transformer networks to graph problems (Dwivedi & Bresson, 2020; Rong et al., 2020; Kreuzer et al., 2021; Ying

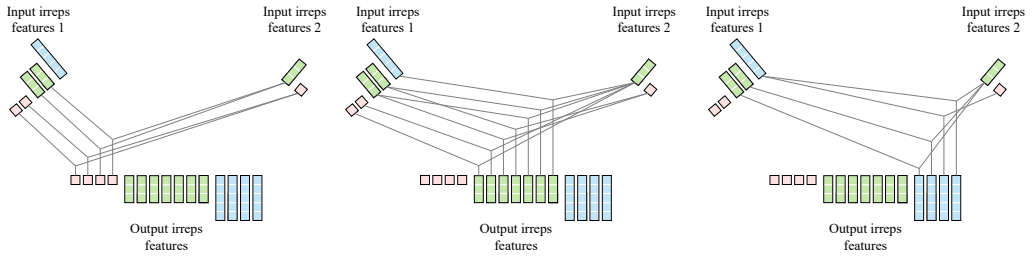

(a) Paths contributing to type-*0* vectors. **(b) Paths contributing to type-*1* vectors.** **(c) Paths contributing to type-*2* vectors.**

Figure 3: **An alternative visualization of the depth-wise tensor product.** We follow the visualization of tensor products in `e3nn` (Geiger et al., 2022) and separate paths into three parts based on the types of output vectors. We note that one vector in the output irreps feature depends only on one vector in each input irreps feature.

et al., 2021; Shi et al., 2022). They adopt dot product attention in Transformers (Vaswani et al., 2017) and propose different approaches to incorporate graph-related inductive biases into their networks. GROVE (Rong et al., 2020) includes additional message passing layers or graph convolutional layers to incorporate local graph structures when calculating attention weights. SAN (Kreuzer et al., 2021) proposes to learn position embeddings of nodes with full Laplacian spectrum. Graphormer (Ying et al., 2021) proposes to encode degree information in centrality embeddings and encode distances and edge features in attention biases. The proposed Equiformer belongs to one of these attempts to generalize standard Transformers to graphs and is dedicated to 3D graphs. To incorporate 3D-related inductive biases, we adopt an equivariant version of Transformers with irreps features and propose novel equivariant graph attention.

C Details of Architecture

C.1 Equivariant Operation Used in Equiformer

We illustrate the equivariant operations used in Equiformer in Fig. 2 and provide an alternative visualization of depth-wise tensor products in Fig. 3.

C.2 Equiformer Architecture

For simplicity and because most works we compare with do not include equivariance to inversion, we adopt $SE(3)$-equivariant irreps features in Equiformer for experiments in the main text and note that $E(3)$-equivariant irreps features can be easily incorporated into Equiformer.

We define architectural hyper-parameters like the number of channels in some layers in Equiformer, which are used to specify the detailed architectures in Sec. D.1, Sec. E.1 and Sec. F.2.

We use d_{embed} to denote embedding dimension, which defines the dimension of most irreps features. Specifically, all irreps features x_i, y_i in Fig. 1 have dimension d_{embed} unless otherwise stated. Besides, we use d_{sh} to represent the dimension of spherical harmonics embeddings of relative positions in all depth-wise tensor products.

For equivariant graph attention in Fig. 1(b), the first two linear layers have the same output dimension d_{embed}. The output dimension of depth-wise tensor products (DTP) are determined by that of input irreps features. Equivariant graph attention consists of h parallel attention functions, and the value vector in each attention function has dimension d_{head}. We refer to h and d_{head} as the number of heads and head dimension, respectively. By default, we set the number of channels in scalar feature $f_{ij}^{(0)}$ to be the same as the number of channels of type-0 or type-$(0, e)$ vectors in v_{ij}. When non-linear messages are adopted in v_{ij}, we set the dimension of output irreps features in gate activation to be $h \times d_{head}$. Therefore, we can use two hyper-parameters h and d_{head} to specify the detailed architecture of equivariant graph attention.

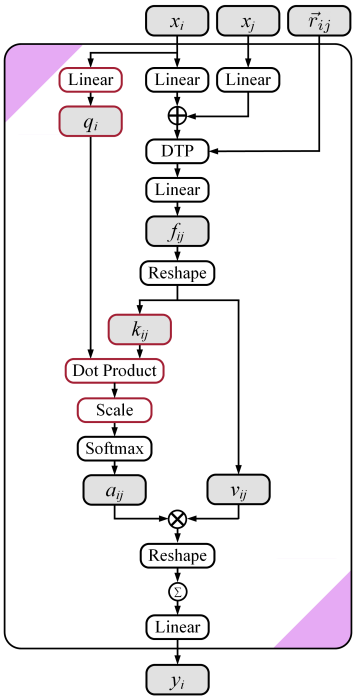

Figure 4: **Architecture of equivariant dot product attention without non-linear message passing.** In this figure, "$\otimes$" denotes multiplication, "$\oplus$" denotes addition, and "DTP" stands for depth-wise tensor product. $\sum$ within a circle denotes summation over all neighbors. Gray cells indicate intermediate irreps features. We highlight the difference of dot product attention from multi-layer perceptron attention in red. Note that key k_{ij} and value v_{ij} are irreps features and therefore f_{ij} in dot product attention typically has more channels than that in multi-layer perceptron attention.

As for feed forward networks (FFNs), we denote the dimension of output irreps features in gate activation as d_{ffn}. The FFN in the last Transformer block has output dimension $d_{feature}$, and we set d_{ffn} of the last FFN, which is followed by output head, to be $d_{feature}$ as well. Thus, two hyper-parameters d_{ffn} and $d_{feature}$ are used to specify architectures of FFNs and the output dimension after Transformer blocks.

Irreps features contain channels of vectors with degrees up to L_{max}. We denote C_L type-L vectors as (C_L, L) and $C_{(L,p)}$ type-(L, p) vectors as $(C_{(L,p)}, L, p)$ and use brackets to represent concatenations of vectors. For example, the dimension of irreps features containing 256 type-0 vectors and 128 type-1 vectors can be represented as $[(256, 0), (128, 1)]$.

C.3 Dot Product Attention

We illustrate the dot product attention without non-linear message passing used in ablation study in Fig. 4. The architecture is adapted from SE(3)-Transformer (Fuchs et al., 2020). The difference from multi-layer perceptron attention lies in how we obtain attention weights a_{ij} from f_{ij}. We split f_{ij} into two irreps features, key k_{ij} and value v_{ij}, and obtain query q_i with a linear layer. Then, we perform scaled dot product (Vaswani et al., 2017) between q_i and k_{ij} for attention weights.

C.4 Discussion on Computational Complexity

We discuss the computational complexity of the proposed equivariant graph attention here.

First, we compare dot product attention with MLP attention when linear messages are used for value v_{ij}. Dot product attention requires taking the dot product of two irreps features, query q_i and key k_{ij}, for attention weights, and both q_i and k_{ij} have the same dimension as value v_{ij}. In contrast, MLP attention uses only scalar features $f_{ij}^{(0)}$ for attention weights. The dimension of scalar features

Hyper-parameters	Value or description
Optimizer	AdamW
Learning rate scheduling	Cosine learning rate with linear warmup
Warmup epochs	5
Maximum learning rate	1.5×10^{-4}, 5×10^{-4}
Batch size	64, 128
Number of epochs	300, 600
Weight decay	0, 5×10^{-3}
Dropout rate	0.0, 0.1, 0.2
Cutoff radius (Å)	5
Number of radial bases	128 for Gaussian radial basis, 8 for radial bessel basis
Hidden sizes of radial functions	64
Number of hidden layers in radial functions	2
	Equiformer
Number of Transformer blocks	6
Embedding dimension d_{embed}	$[(128, 0), (64, 1), (32, 2)]$
Spherical harmonics embedding dimension d_{sh}	$[(1, 0), (1, 1), (1, 2)]$
Number of attention heads h	4
Attention head dimension d_{head}	$[(32, 0), (16, 1), (8, 2)]$
Hidden dimension in feed forward networks d_{ffn}	$[(384, 0), (192, 1), (96, 2)]$
Output feature dimension $d_{feature}$	$[(512, 0)]$
	$E(3)$-Equiformer
Number of Transformer blocks	6
Embedding dimension d_{embed}	$[(128, 0, e), (32, 0, o), (32, 1, e), (32, 1, o), (16, 2, e), (16, 2, o)]$
Spherical harmonics embedding dimension d_{sh}	$[(1, 0, e), (1, 1, o), (1, 2, e)]$
Number of attention heads h	4
Attention head dimension d_{head}	$[(32, 0, e), (8, 0, o), (8, 1, e), (8, 1, o), (4, 2, e), (4, 2, o)]$
Hidden dimension in feed forward networks d_{ffn}	$[(384, 0, e), (96, 0, o), (96, 1, e), (96, 1, o), (48, 2, e), (48, 2, o)]$
Output feature dimension $d_{feature}$	$[(512, 0, e)]$

Table 8: **Hyper-parameters for QM9 dataset.** We denote C_L type-L vectors as (C_L, L) and $C_{(L,p)}$ type-(L, p) vectors as $(C_{(L,p)}, L, p)$ and use brackets to represent concatenations of vectors.

$f_{ij}^{(0)}$ is the same as that of the scalar part of v_{ij}. Therefore, MLP attention generates less and smaller intermediate features for attention weights and is faster than dot product attention.

Second, compared to linear messages, using non-linear messages increases the number of tensor product operations from 1 to 2. Since tensor products are compute-intensive, this inevitably increases training and inference time.

Please refer to Sec. D.1 and Sec. F.2 for the exact numbers of training time on QM9 and OC20.

D Details of Experiments on QM9

D.1 Training Details

We use the same data partition as TorchMD-NET (Thölke & Fabritiis, 2022). For the task of U, U_0, G, and H, where single-atom reference values are available, we subtract those reference values from ground truth. For other tasks, we normalize ground truth by subtracting mean and dividing by standard deviation.

We train Equiformer with 6 blocks with $L_{max} = 2$. We choose Gaussian radial basis (Schütt et al., 2017; Shuaibi et al., 2021; Klicpera et al., 2021; Shi et al., 2022) for the first six tasks in Table 1 and radial Bessel basis (Gasteiger et al., 2020b;a) for the others. We apply dropout (Srivastava et al., 2014) to attention weights a_{ij}. The dropout rate is 0.0 for the tasks of G, H, U and U_0, is 0.1 for the task of R^2 and is 0.2 for others. Since the tasks of G, H, U, and U_0 require longer training, we use slightly different hyper-parameters. The number of epochs is 600 for the tasks of G, H, U, and U_0 and is 300 for others. The learning rate is 1.5×10^{-4} for the tasks of G, H, U, and U_0 and is 5×10^{-4} for others. The batch size is 64 for the tasks of G, H, U, and U_0 and is 128 for others. The weight decay is 0 for the tasks of G, H, U, and U_0 and is 5×10^{-3} for others. Table 8 summarizes

the hyper-parameters for the QM9 dataset. The detailed description of architectural hyper-parameters can be found in Sec. C.2.

We use one A6000 GPU with 48GB to train each model and summarize the computational cost of training for one epoch as follows. Training $E(3)$-Equiformer in Table 9 for one epoch takes about 16.3 minutes. The time of training Equiformer, Equiformer with linear messages (indicated by Index 2 in Table 6), and Equiformer with linear messages and dot product attention (indicated by Index 3 in Table 6) for one epoch is 12.1 minutes, 7.2 minutes and 7.8 minutes, respectively.

D.2 Comparison between $SE(3)$ and $E(3)$ Equivariance

We train two versions of Equiformers, one with $SE(3)$-equivariant features denoted as "Equiformer" and the other with $E(3)$-equivariant features denoted as "$E(3)$-Equiformer", and we compare them in Table 9. As for Table 1, we compare "Equiformer" with other works since most of them do not include equivariance to inversion.

Methods	Task Units	α bohr^3	$\Delta\varepsilon$ meV	$\varepsilon_{\text{HOMO}}$ meV	$\varepsilon_{\text{LUMO}}$ meV	μ D	C_ν cal/mol K	Training time (minutes/epoch)	Number of parameters
Equiformer		.046	30	15	14	.011	.023	12.1	3.53M
$E(3)$-Equiformer		.045	30	15	14	.012	.023	16.3	3.28M

Table 9: **Ablation study of $SE(3)$/$E(3)$ equivariance on QM9 testing set.** "Equiformer" operates on $SE(3)$-equivariant features while "$E(3)$-Equiformer" uses $E(3)$-equivariant features. Including inversion achieves similar performance.

D.3 Comparison of Training Time and Numbers of Parameters

We compare training time and numbers of parameters between SEGNN (Brandstetter et al., 2022), TorchMD-NET (Thölke & Fabritiis, 2022) and Equiformer and summarize the results in Table 10. Training Equiformer for 300 epochs and for 600 epochs takes 61 and 122 GPU-hours, respectively.

Compared to SEGNN, which is written with the same `e3nn` library (Geiger et al., 2022), Equiformer with MLP attention and non-linear message is faster. Although Equiformer has more channels and more parameters, the training time is comparable. The reasons are as follows. Equiformer uses more efficient depth-wise tensor products (DTP), where one output channel depends on only one input channel. SEGNN uses more compute-intensive fully connected tensor products (FCTP), where one output channel depends on all input channels. Besides, SEGNN uses 4 FCTPs in each message passing block while Equiformer uses only 2 DTPs in each block.

Compared to TorchMD-NET, which is trained for 3000 epochs, Equiformer achieves competitve results after trained for 300 or 600 epochs. Equiformer takes more time for each epoch since Equiformer uses more expressive non-linear messages, which compared to linear messages used in other equivariant Transformers, doubles the number of tensor products and therefore almost doubles the training time. Moreover, Equiformer incorporates tensors of higher degrees (e.g., $L_{max} = 2$), which improves performance but slows down the training.

E Details of Experiments on MD17

E.1 Training Details

We train Equiformer with 6 blocks with $L_{max} = 2$ and 3. We choose the radial basis function used by PhysNet (Unke & Meuwly, 2019). We do not apply dropout to attention weights a_{ij}. For Equiformer with $L_{max} = 2$, the learning rate is 1×10^{-4} for benzene and is 5×10^{-4} for others. The batch size is 8, and the number of epochs is 1500. The model has about 3.50M parameters. For Equiformer with $L_{max} = 3$, the learning rate is 1×10^{-4} for benzene and is 2×10^{-4} for others. The batch size is 5, and the number of epochs is 2000. The model has about 5.50M parameters. Table 11 summarizes the hyper-parameters for the MD17 dataset. The detailed description of architectural hyper-parameters can be found in Sec. C.2.

We use one A5000 GPU with 24GB to train different models for each molecule. Training Equiformer with $L_{max} = 2$ takes about 15.4 hours, and training Equiformer with $L_{max} = 3$ takes about 54.4 hours.

Methods	Number of parameters	Training time (GPU-hours)
SEGNN (Brandstetter et al., 2022)	1.03M	81
TorchMD-NET (Thölke & Fabritiis, 2022)	6.86M	92
Equiformer	3.53M	61

Table 10: **Comparison of training time and numbers of parameters for QM9 dataset.**

Hyper-parameters	Value or description
Optimizer	AdamW
Learning rate scheduling	Cosine learning rate with linear warmup
Warmup epochs	10
Maximum learning rate	1×10^{-4}, 2×10^{-4}, 5×10^{-4}
Batch size	5, 8
Number of epochs	1500, 2000
Weight decay	1×10^{-6}
Dropout rate	0.0
Weight for energy loss	1
Weight for force loss	100
Cutoff radius (Å)	5
Number of radial bases	32
Hidden sizes of radial functions	64
Number of hidden layers in radial functions	2
Equiformer ($L_{max} = 2$)	
Number of Transformer blocks	6
Embedding dimension d_{embed}	$[(128, 0), (64, 1), (32, 2)]$
Spherical harmonics embedding dimension d_{sh}	$[(1, 0), (1, 1), (1, 2)]$
Number of attention heads h	4
Attention head dimension d_{head}	$[(32, 0), (16, 1), (8, 2)]$
Hidden dimension in feed forward networks d_{ffn}	$[(384, 0), (192, 1), (96, 2)]$
Output feature dimension $d_{feature}$	$[(512, 0)]$
Equiformer ($L_{max} = 3$)	
Number of Transformer blocks	6
Embedding dimension d_{embed}	$[(128, 0), (64, 1), (64, 2), (32, 3)]$
Spherical harmonics embedding dimension d_{sh}	$[(1, 0), (1, 1), (1, 2), (1, 3)]$
Number of attention heads h	4
Attention head dimension d_{head}	$[(32, 0), (16, 1), (16, 2), (8, 3)]$
Hidden dimension in feed forward networks d_{ffn}	$[(384, 0), (192, 1), (192, 2), (96, 3)]$
Output feature dimension $d_{feature}$	$[(512, 0)]$

Table 11: **Hyper-parameters for MD17 dataset.** We denote C_L type-L vectors as (C_L, L) and $C_{(L,p)}$ type-(L, p) vectors as $(C_{(L,p)}, L, p)$ and use brackets to represent concatenations of vectors.

E.2 Additional Comparison to TorchMD-NET

Since TorchMD-NET (Thölke & Fabritiis, 2022) is also an equivariant Transformer but uses dot product attention instead of the proposed equivariant graph attention, we provide additional comparisons in Table 12. For each molecule, we adjust the ratio of the weight for force loss to the weight for energy loss so that Equiformer with $L_{max} = 2$ can achieve lower MAE for both energy and forces.

E.3 Comparison of Training Time and Numbers of Parameters

We compare training time and number of parameters between NequIP (Batzner et al., 2022) and Equiformer and summarize the results in Table 13. Since NequIP does not report the number of epochs, we compare the time spent for each epoch and note that NequIP is trained for more than 1000 epochs. Equiformer with $L_{max} = 2$ is faster than NequIP with $L_{max} = 3$ since smaller L_{max} is used. Moreover, Equiformer with $L_{max} = 2$ achieves overall better results as we use equivariant graph attention instead of linear convolution used by NequIP. When increasing L_{max} from 2 to 3, Equiformer achieves better results than NequIP for most molecules. However, the training time is longer than NequIP since we use 2 tensor product operations in each equivariant graph attention instead of 1 tensor product in each linear convolution.

	Aspirin		Benzene		Ethanol		Malonaldehyde		Naphthalene		Salicylic acid		Toluene		Uracil	
Methods	energy	forces	energy	forces	energy	forces	energy	forces	energy	forces	energy	forces	energy	forces	energy	forces
TorchMD-NET	**5.3**	11.0	2.5	8.5	2.3	4.7	3.3	7.3	**3.7**	2.6	**4.0**	5.6	**3.2**	2.9	**4.1**	4.1
Equiformer ($L_{max} = 2$)	**5.3**	**7.2**	**2.2**	**6.6**	**2.2**	**3.1**	**3.3**	**5.8**	**3.7**	**2.1**	**4.0**	**5.3**	**3.2**	**2.4**	4.2	**3.7**

Table 12: **Additional comparison to TorchMD-Net (Thölke & Fabritiis, 2022) on MD17 dataset.** Energy and force are in units of meV and meV/Å.

Methods	Number of parameters	Training time (secs/epoch)
NequIP ($L_{max} = 3$) (Batzner et al., 2022)	2.97M	48.7
Equiformer ($L_{max} = 2$)	3.50M	36.9
Equiformer ($L_{max} = 3$)	5.50M	98.0

Table 13: **Comparison of training time and numbers of parameters for MD17 dataset.**

F Details of Experiments on OC20

F.1 Detailed Description of OC20 Dataset

The dataset consists of larger atomic systems, each composed of a molecule called adsorbate placed on a slab called catalyst. Each input contains more atoms and more diverse atom types than QM9 and MD17. The average number of atoms in a system is more than 70, and there are over 50 atom species. The goal is to understand interaction between adsorbates and catalysts through relaxation. An adsorbate is first placed on top of a catalyst to form initial structure (IS). The positions of atoms are updated with forces calculated by density function theory until the system is stable and becomes relaxed structure (RS). The energy of RS, or relaxed energy (RE), is correlated with catalyst activity and therefore a metric for understanding their interaction. We focus on the task of initial structure to relaxed energy (IS2RE), which predicts relaxed energy (RE) given an initial structure (IS). There are 460k, 100k and 100k structures in training, validation, and testing sets, respectively.

F.2 Training Details

IS2RE without Node-Level Auxiliary Task. We use hyper-parameters similar to those for QM9 dataset and summarize in Table 14. For ablation study in Sec. 5.4, we use a smaller learning rate 1.5×10^{-4} for DP attention as this improves the performance. The detailed description of architectural hyper-parameters can be found in Sec. C.2.

IS2RE with IS2RS Node-Level Auxiliary Task. We increase the number of Transformer blocks to 18 as deeper networks can benefit more from IS2RS node-level auxiliary task (Godwin et al., 2022). We follow the same hyper-parameters in Table 14 except that we increase maximum learning rate to 5×10^{-4} and set $d_{feature}$ to $[(512, 0), (256, 1)]$. Inspired by Graphormer (Shi et al., 2022), we add an extra equivariant graph attention module after the last layer normalization to predict relaxed structures and use a linearly decayed weight for loss associated with IS2RS, which starts at 15 and decays to 1. For Noisy Nodes (Godwin et al., 2022) data augmentation, we first interpolate between initial structure and relaxed structure and then add Gaussian noise as described by Noisy Nodes (Godwin et al., 2022). When Noisy Nodes data augmentation is used, we increase the number of epochs to 40.

We use two A6000 GPUs, each with 48GB, to train models when IS2RS is not included during training. Training Equiformer and $E(3)$-Equiformer in Table 16 takes about 43.6 and 58.3 hours. Training Equiformer with linear messages (indicated by Index 2 in Table 7) and Equiformer with linear messages and dot product attention (indicated by Index 3 in Table 7) takes 30.4 hours and 33.1 hours, respectively. We use four A6000 GPUs to train Equiformer models when IS2RS node-level auxiliary task is adopted during training. Training Equiformer without Noisy Nodes data augmentation takes about 3 days and training with Noisy Nodes takes 6 days. We note that the proposed Equiformer in Table 5 achieves competitive results even with much less computation. Specifically, training "Equiformer + Noisy Nodes" takes about 24 GPU-days when A6000 GPUs are used. The training time of "GNS + Noisy Nodes" (Godwin et al., 2022) is 56 TPU-days. "Graphormer" (Shi et al., 2022) uses ensemble of 31 models and requires 372 GPU-days to train all models when A100 GPUs are used.

Hyper-parameters	Value or description
Optimizer	AdamW
Learning rate scheduling	Cosine learning rate with linear warmup
Warmup epochs	2
Maximum learning rate	2×10^{-4}
Batch size	32
Number of epochs	20
Weight decay	1×10^{-3}
Dropout rate	0.2
Cutoff radius (Å)	5
Number of radial basis	128
Hidden size of radial function	64
Number of hidden layers in radial function	2
Equiformer	
Number of Transformer blocks	6
Embedding dimension d_{embed}	$[(256, 0), (128, 1)]$
Spherical harmonics embedding dimension d_{sh}	$[(1, 0), (1, 1)]$
Number of attention heads h	8
Attention head dimension d_{head}	$[(32, 0), (16, 1)]$
Hidden dimension in feed forward networks d_{ffn}	$[(768, 0), (384, 1)]$
Output feature dimension $d_{feature}$	$[(512, 0)]$
$E(3)$-Equiformer	
Number of Transformer blocks	6
Embedding dimension d_{embed}	$[(256, 0, e), (64, 0, o), (64, 1, e), (64, 1, o)]$
Spherical harmonics embedding dimension d_{sh}	$[(1, 0, e), (1, 1, o)]$
Number of attention heads h	8
Attention head dimension d_{head}	$[(32, 0, e), (8, 0, o), (8, 1, e), (8, 1, o)]$
Hidden dimension in feed forward networks d_{ffn}	$[(768, 0, e), (192, 0, o), (192, 1, e), (192, 1, o)]$
Output feature dimension $d_{feature}$	$[(512, 0, e)]$

Table 14: **Hyper-parameters for OC20 dataset under the setting of training without IS2RS auxiliary task.** We denote C_L type-L vectors as (C_L, L) and $C_{(L,p)}$ type-(L, p) vectors as $(C_{(L,p)}, L, p)$ and use brackets to represent concatenations of vectors.

	Energy MAE (eV) ↓					EwT (%) ↑				
Methods	ID	OOD Ads	OOD Cat	OOD Both	Average	ID	OOD Ads	OOD Cat	OOD Both	Average
SchNet (Schütt et al., 2017)†	0.6465	0.7074	0.6475	0.6626	0.6660	2.96	2.22	3.03	2.38	2.65
DimeNet++ (Gasteiger et al., 2020a)†	0.5636	0.7127	0.5612	0.6492	0.6217	4.25	2.48	4.40	2.56	3.42
GemNet-T (Klicpera et al., 2021)†	0.5561	0.7342	0.5659	0.6964	0.6382	4.51	2.24	4.37	2.38	3.38
SphereNet (Liu et al., 2022)	0.5632	0.6682	0.5590	0.6190	0.6024	4.56	2.70	4.59	2.70	3.64
(S)EGNN (Brandstetter et al., 2022)	0.5497	0.6851	0.5519	0.6102	0.5992	4.99	2.50	4.71	2.88	3.77
SEGNN (Brandstetter et al., 2022)	0.5310	0.6432	0.5341	0.5777	0.5715	**5.32**	2.80	4.89	**3.09**	**4.03**
Equiformer	**0.5088**	**0.6271**	**0.5051**	**0.5545**	**0.5489**	4.88	**2.93**	**4.92**	2.98	3.93

Table 15: **Results on OC20 IS2RE validation set.** † denotes results reported by Liu et al. (2022).

F.3 Results on IS2RE Validation Set

For completeness, we report the results of Equiformer on the validation set in Table 15.

F.4 Comparison between $SE(3)$ and $E(3)$ Equivariance

We train two versions of Equiformers, one with $SE(3)$-equivariant features denoted as "Equiformer" and the other with $E(3)$-equivariant features denoted as "$E(3)$-Equiformer", and we compare them in Table 16. Including inversion improves the MAE results on ID and OOD Cat sub-splits but degrades the performance on the other sub-splits. Overall, using $E(3)$-equivariant features results in slightly inferior performance. We surmise the reasons are as follows. First, inversion might not be the key bottleneck. Second, including inversion would break type-1 vectors into two parts, type-$(1, e)$ and type-$(1, o)$ vectors. They are regarded as different types in equivariant linear layers and layer normalizations, and therefore, the directional information captured in these two types of vectors can only exchange in depth-wise tensor products. Third, we mainly tune hyper-parameters for Equiformer with $SE(3)$-equivariant features, and it is possible that using $E(3)$-equivariant features would favor different hyper-parameters.

Methods	Energy MAE (eV) ↓					EwT (%) ↑					Training time (minutes/epoch)	Number of parameters
	ID	OOD Ads	OOD Cat	OOD Both	Average	ID	OOD Ads	OOD Cat	OOD Both	Average		
Equiformer	0.5088	0.6271	0.5051	0.5545	0.5489	4.88	2.93	4.92	2.98	3.93	130.8	9.12M
$E(3)$-Equiformer	0.5035	0.6385	0.5034	0.5658	0.5528	5.10	2.98	5.10	3.02	4.05	174.9	8.77M

Table 16: **Ablation study of $SE(3)$/$E(3)$ equivariance on OC20 IS2RE validation set.** "Equiformer" operates on $SE(3)$-equivariant features while "$E(3)$-Equiformer" uses $E(3)$-equivariant features.

Methods	Number of parameters	Training time (GPU-hours)
SEGNN (Brandstetter et al., 2022)	4.21M	79
Equiformer	9.12M	87

Table 17: **Comparison of training time and numbers of parameters for OC20 dataset.**

For Table 15, 3, 4, and 5, we compare "Equiformer" with other works since most of them do not include equivariance to inversion.

F.5 Comparison of Training Time and Numbers of Parameters

We compare training time and number of parameters between SEGNN (Brandstetter et al., 2022) and Equiformer when IS2RS auxiliary task is not adopted during training and summarize the results in Table 17. Equiformer achieves better results with comparable training time. Please refer to Sec. D.3 for a detailed discussion.

The comparison of training time when IS2RS auxiliary task is adopted can be found in Table 5.

F.6 Error Distributions

We plot the error distributions of different Equiformer models on different sub-splits of OC20 IS2RE validation set in Fig. 5. For each curve, we sort the absolute errors in ascending order for better visualization and have a few observations. First, for each sub-split, there are always easy examples, for which all models achieve significantly low errors, and hard examples, for which all models have high errors. Second, the performance gains brought by different models are non-uniform among different sub-splits. For example, using MLP attention and non-linear messages improves the errors on the ID sub-split but is not that helpful on the OOD Ads sub-split. Third, when IS2RS node-level auxiliary task is not included during training, using stronger models mainly improves errors that are beyond the threshold of 0.02 eV, which is used to calculate the metric of energy within threshold (EwT). For instance, on the OOD Both sub-split, using non-linear messages, which corresponds to red and purple curves, improves the absolute errors for the 15000th through 20000th examples. However, the improvement in MAE does not translate to that in EwT as the errors are still higher than the threshold of 0.02 eV. This explains why using non-linear messages in Table 7 improves MAE from 0.5657 to 0.5545 but results in almost the same EwT.

G Limitations

We discuss several limitations of the proposed Equiformer and equivariant graph attention below.

First, Equiformer is based on irreducible representations (irreps) and therefore can inherit the limitations common to all equivariant networks based on irreps and the library `e3nn` (Geiger et al., 2022). For example, using higher degrees L can result in larger features and using tensor products can be compute-intensive. Part of the reasons that tensor products can be computationally expensive are that the kernels have not been heavily optimized and customized as other operations in common libraries like PyTorch (Paszke et al., 2019). But this is the issue related to software, not the design of networks. While tensor products of irreps naively do not scale well, if all possible interactions and paths are considered, some paths in tensor products can also be pruned for computational efficiency. We leave these potential efficiency gains to future work and in this work focus on general equivariant attention if all possible paths up to L_{max} in tensor products are allowed.

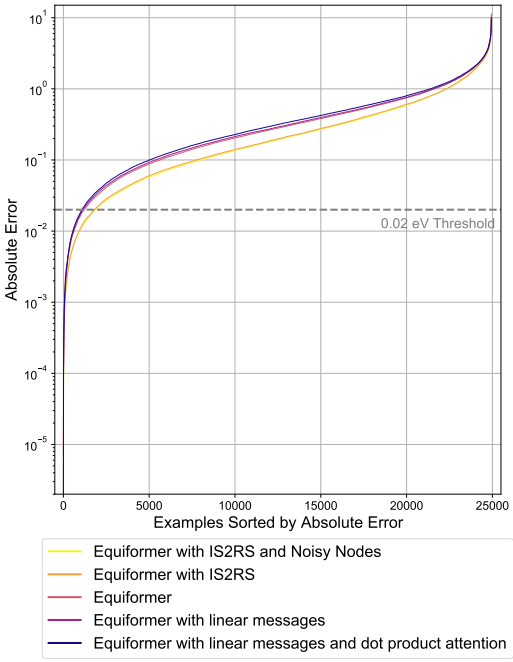

(a) **ID sub-split.**

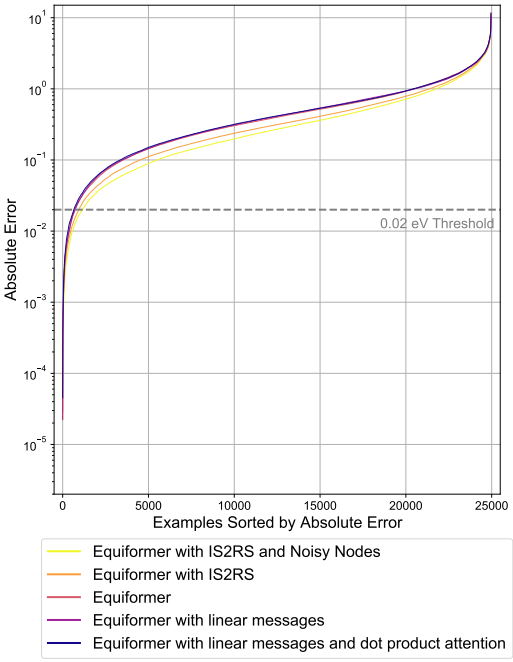

(b) **OOD Ads sub-split.**

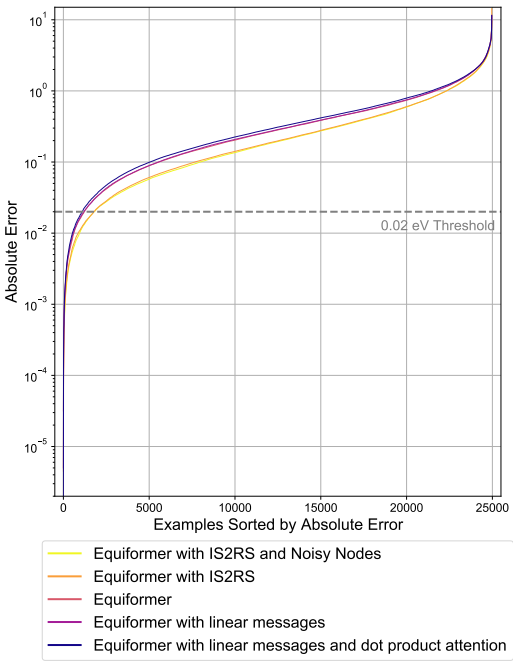

(c) **OOD Cat sub-split.**

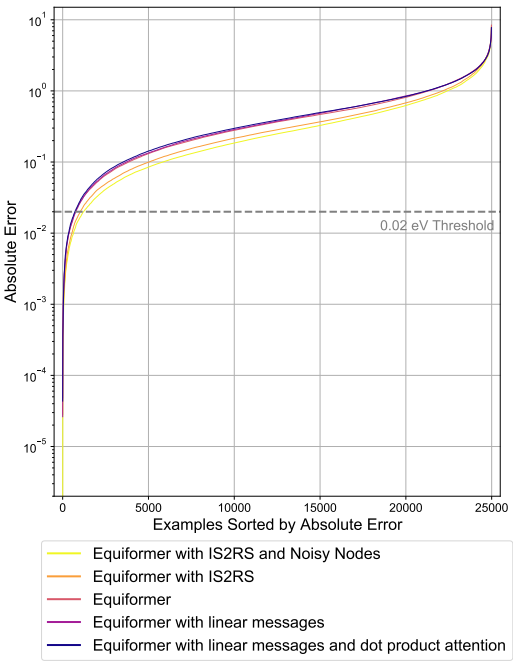

(d) **OOD Both sub-split.**

Figure 5: **Error distributions of different Equiformer models on different sub-splits of OC20 IS2RE validation set.**

Second, the improvement of the proposed equivariant graph attention can depend on tasks and datasets. For QM9, MLP attention improves not significantly upon dot product attention as shown in Table 6. We surmise that this is because QM9 contains less atoms and less diverse atom types and therefore linear attention is enough. For OC20, MLP attention clearly improves upon dot product attention as shown in Table 7. Non-linear messages improve upon linear ones for the two datasets.

Third, equivariant graph attention requires more computation than typical graph convolution. It includes one softmax operation and thus requires one additional sum aggregation compared to typical message passing. For non-linear message passing, it increases the number of tensor products from one to two and requires more computation. We note that if there is a constraint on training budget, using stronger attention (i.e., MLP attention and non-linear messages) would not always be optimal because for some tasks or datasets, the improvement is not that significant and using stronger attention can slow down training.

Fourth, the proposed attention has complexity proportional to the products of numbers of channels and numbers of edges since the the attention is restricted to local neighborhoods. In the context of 3D atomistic graphs, the complexity is the same as that of messages and graph convolutions. However, in other domains like computer vision, the memory complexity of convolution is proportional to the number of pixels or nodes, not that of edges. Therefore, it would require further modifications in order to use the proposed attention in other domains.